Design, Analysis, and Control of Switched Supercapacitor Banks for E-transportation Electric Energy Storage Systems

by

Yashwanth Dasari

A thesis submitted to the
School of Graduate and Postdoctoral Studies in partial
fulfillment of the requirements for the degree of

Master of Applied Science

in the

Faculty of Engineering and Applied Science
Department of Electrical, Computer, and Software Engineering
University of Ontario Institute of Technology (Ontario Tech University)
Oshawa, Ontario, Canada

July 2020

Thesis Examination Information

Submitted by: **Yashwanth Dasari**

Master of Applied Science in **Electrical and Computer Engineering**

Thesis title: Design, Analysis, and Control of Switched Supercapacitor Banks for E-transportation Electric Energy Storage Systems

An oral defense of this thesis took place on 17 July 2020, in front of the following examining committee:

Examining Committee:

Chair of Examining Committee	: Dr. Ying Wang
Research Supervisor	: Dr. Sheldon Williamson
Examining Committee Member	: Dr. Mohamed Youssef
Thesis Examiner	: Dr. Xianke Lin

The above committee determined that the thesis is acceptable in form and content and that a satisfactory knowledge of the field covered by the thesis was demonstrated by the candidate during an oral examination. A signed copy of the Certificate of Approval is available from the School of Graduate and Postdoctoral Studies.

Abstract

The hybridization of supercapacitors (SCs) with batteries in electric vehicles (EVs) improves the battery life, acceleration, and driving range. However, the efficiency of the power interface that unites the batteries and SCs are affected due to wide voltage variations at the SC bank terminals. Moreover, the SC bank offers low storage that restricts them from serving a continuous series of transient load demands on a single charge.

A novel bank switching architecture for SCs is introduced to enhance the power delivery duration and energy utilization of SCs with controlled terminal voltage variations. A simple transition control strategy is proposed to effectively switch the SCs. The efficacy of the proposed work is validated using simulations and experimental studies on a laboratory-developed prototype. Furthermore, the suitability of the proposed SC bank in HESS for an EV is verified with four standard driving cycles, in terms of voltage variations, and depth of discharge.

Keywords: Bank switching; dc-dc power converter; electric vehicles; hybrid energy storage systems; supercapacitors.

Author's Declaration

I hereby declare that this thesis consists of original work of which I have authored. This is a true copy of the thesis, including any required final revisions, as accepted by my examiners.

I authorize the University of Ontario Institute of Technology (Ontario Tech University) to lend this thesis to other institutions or individuals for the purpose of scholarly research. I further authorize the University of Ontario Institute of Technology (Ontario Tech University) to reproduce this thesis by photocopying or by other means, in total or in part, at the request of other institutions or individuals for the purpose of scholarly research. I understand that my thesis will be made electronically available to the public.

_____ YASHWANTH DASARI

Statement of Contributions

A new bank switching architecture for supercapacitors is introduced in this thesis. The proposed concept is validated by conducting related experiments and simulation studies.

The work described in Chapter 3 is published as:

- **Y. Dasari**, D. Ronanki, and S. S. Williamson, "Novel Bank Switching of Supercapacitors with Enhanced Energy Utilization for Electric Vehicular Applications," in *Proc. IEEE Transportation Electrification Conference and Expo (ITEC)*, Chicago, Illinois, June 2020, pp. 484–488.

The part of work presented in Chapters 2, 3, and 4 are accepted for publication as:

- **Y. Dasari**, D. Ronanki, and S. S. Williamson, "Power Management of Supercapacitors using Auxiliary Bank Switching for Hybrid Energy Storage Systems," in *Proc. IEEE Energy Conversion Congress and Exposition (ECCE)*, Detroit, MI, USA, Sept. 2020.

The part of work presented in Chapters 1, and 2 are accepted for publication as:

- **Y. Dasari**, D. Ronanki, and S. S. Williamson, "Performance Evaluation of Supercapacitor Bank Switching Architectures for Pulsed Power Loads," in *Proc. IECON 2020 - 46th Annual Conference of the IEEE Industrial Electronics Society*, Singapore, Oct. 2020.

The portion of work described in Chapters 2, 3, 4, and 5 is published as:

- **Y. Dasari**, D. Ronanki, and S. S. Williamson, "A Simple Three-level Switching Architecture to Enhance the Power Delivery Duration of Supercapacitor Banks in Electrified Transportation," *IEEE Transactions on Transportation Electrification*, June 2020, doi: 10.1109/TTE.2020.3001024. (Early Access).

I performed the majority of the analysis, testing, and validation for the proposed configuration along with drafting the manuscripts. Moreover, I have used the standard referencing practices to acknowledge the ideas, research techniques, and other materials. I hereby certify that I am the sole source of the inventive knowledge described in this thesis.

Acknowledgments

Firstly, I would like to express my heartfelt gratitude to my supervisor **Prof. Sheldon S. Williamson** for giving me an opportunity to work in the Smart transportation electrification (STEER) group. Working under him as a Graduate Research Assistant had always been a great delight and I take this opportunity to recognize all the timely help rendered by him. I would like to thank him for his continuous encouragement, guidance, and support throughout my research work. I convey my admiration for him in suggesting various interesting ideas during the course of the project. I sincerely thank him for providing me with the opportunities to engage in seminars, conventions, and other official conversations which helped me to meet several individuals and acquire knowledge in diverse fields.

Besides, I convey my humble gratitude to **Dr. Deepak Ronanki** for his valuable guidance and inputs which helped me complete the project. His astute comments helped me perform in-depth investigations in my research and established the path to move forward during the bottleneck situations. I extend my thanks to him for sharing his knowledge and helping me learn new tools which enabled me to grow as a skilled researcher.

Lastly, I would like to thank my parents for providing their enormous love, strength, and support throughout this endeavour. Their aid and motivation that helped me develop self-confidence during the woeful and challenging situations. A special thanks to my younger brother for being on my side in all my achievements and failures.

Dedicated to my family

Thank you, Dad and Mom, for all your love and support.

Table of Contents

List of Tables

List of Figures

List of Abbreviations

SC	Supercapacitor
EDLC	Electric double-layer capacitor
ESR	Equivalent series resistance
ESS	Energy storage system
HESS	Hybrid energy storage system
EV	Electric vehicle
HEV	Hybrid electric vehicle
PHEV	Plug-in hybrid electric vehicle
Li-ion	Lithium-Ion
SoC	State of charge
SoH	State of health
DoD	Depth of discharge
CC-CV	Constant current - Constant voltage
FC	Fuel cells
MOSFET	Metal-Oxide-Semiconductor Field-Effect Transistor
PI	Proportional-Integral
CCM	Continuous conduction mode
UDDS	Urban Dynamometer Driving Schedule
HWFET	Highway Fuel Economy Test
NEDC	New European Driving Cycle
LPF	Lowpass filter

List of Symbols

λ	Battery Capacity	Ah
C	Capacitance	F
Q	Charge	C
E	Energy	J
η	Efficiency	%
V	Voltage	V
R	Resistor	Ω
I	Current	A
L	Inductor	H
f	Frequency	Hz
P	Power	W
M	Mass	Kg
A	Area	m^2
d	Diameter	m
v	Velocity	m/s

Chapter 1

Introduction

1.1. Background

Battery operated EVs had been introduced at the beginning of the 19th century preceding the invention of internal combustion vehicles. However, gasoline vehicles had become increasingly popular because of their high reliability and mileage. As per Canada's greenhouse gas emissions executive summary of 2017, the transportation sector is one of the major sources for emitting greenhouse gases into the atmosphere [1] as shown in Figure 1.1. Considering the adverse effects of exhaust emissions, the automotive industry is moving towards greener transportation by deploying EVs, HEVs, and PHEVs to rescue the atmosphere from greenhouse gas emissions.

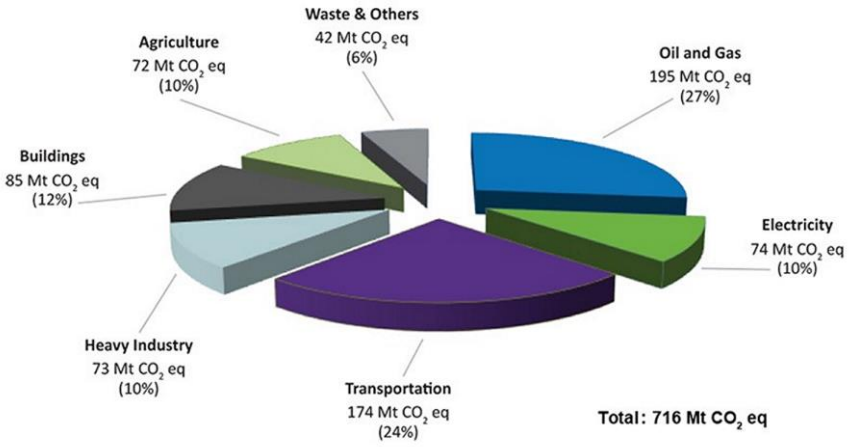

Figure 1.1. Canada's greenhouse gas emissions by economic sector 2017 [1].

1.2. Electric Energy Storage

Energy storage is an essential element in several applications such as cellular phones, smart wearables, and other electric mobility devices. Batteries offer high specific energy with an extended life span. Hence, these are widely used in EVs as a fundamental energy storage device. Besides, there are other sources such as SCs, fly wheel-based storage, pumped-hydro, and FC technology as an ESS for electrified transportation.

1.2.1. Battery

In recent times, batteries are evolved as one of the most promising energy storage devices that are appropriate for long term power supply and storage. These are extensively used for voltage regulation and frequency control in various load applications [2]. Typically, batteries are categorized as primary and secondary storage units. Primary batteries are non-rechargeable and discarded after their first usage. Whereas the secondary batteries are rechargeable and offer high energy densities at constant power loads [3]. Li-ion batteries are one of the mature forms of secondary ESSs which are widely used in automotive drive train and aerospace applications due to their high performance, low self-discharge rates, high storage capacity with an exceptional cycle life compared to the other battery technology [4].

Usually, Li-ion batteries offer high charge/discharge efficiency at a wider temperature range with good specific energy density ranging at 230 Wh/kg [5]. However, few parameters affect the capacity of a battery such as its operating temperature, high discharge rates, and storage conditions [6]. As the batteries have nonlinear behavior, proper estimation of the SoH and SoC are required to analyze its dynamic nature during charge and discharge operations. When a battery is discharged at higher currents, the internal resistance of the cell increases that affect the overall capacity. Moreover, the temperature is one of the major factors to be considered when it comes to the safety and reliability of a battery. The capacity of a Li-ion cell is varied and highly dependant on its operating temperature [7]. The active chemicals of the cell break down at extremely high temperatures and the freezing of electrolyte occurs at extremely low temperatures. Thus, it results in the permanent depreciation of the cell capacity.

The charging of a Li-ion battery is performed using various approaches such as multistage charging, and pulse charging. Among them, CC-CV is chosen as an efficient method in terms of ease implementation and low cost [8]. Moreover, this algorithm has fewer computational steps with reduced hardware complexity. At first, the constant current is supplied to the battery until its corresponding terminal voltage reaches the maximum voltage (V_{max}). At this point, the current source is disconnected, and the constant voltage is supplied to the battery until the current reaches the lower value. consequently, the SoC of

the battery raises from 0% to 100%. The charging behavior of a Li-ion battery using the CC-CV approach is shown in Figure 1.2.

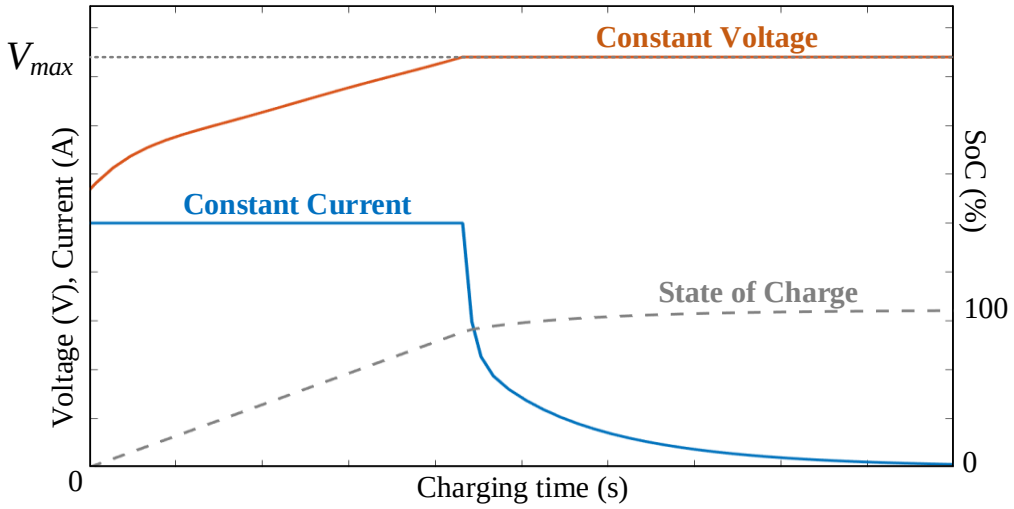

Figure 1.2. CC-CV charging of the Li-ion battery.

The charge and discharge curves of the Li-ion batteries are exponential and deliver stable power to the load for a longer duration. The charge and discharge characteristics of a Li-ion cell are shown in Figure 1.3. During charging, the cell voltage is raised from the cut-off voltage (V_{cutt}) to its maximum voltage (V_{max}). Likewise, the cell voltage is exponentially reduced from V_{max} to V_{cutt}. The Li-ion cell is inoperative when it is discharged till V_{min}. Thus, it is not recommended to deep discharge a Li-ion cell [9].

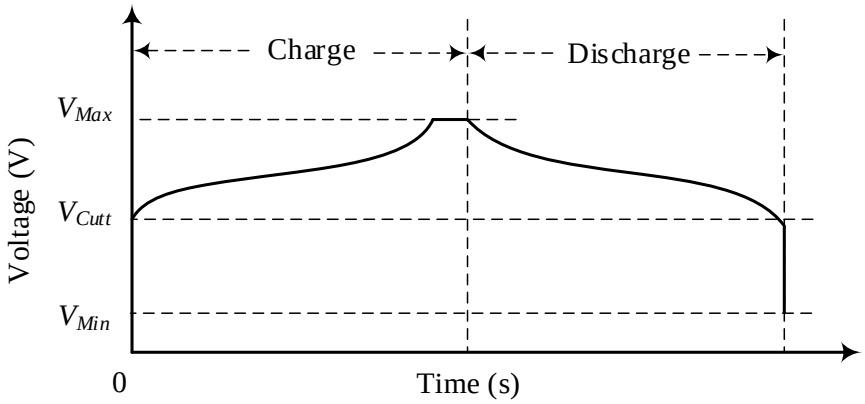

Figure 1.3. Charge and discharge characteristics of a Li-ion Battery [9].

The overall capacity (λ) of a Li-ion battery is estimated using Peukert's equation derived from the constant current approach method [10] i.e. given in (1.1), Where t_{cutt} is the cut-off time in hours, I is the constant discharge current and n is the Peukert's constant which accounts for the intrinsic losses of a battery during charge and discharge operations.

$$\lambda = I_n * t_{cutt} \tag{1.1}$$

1.2.2. Supercapacitors

SCs are well known for their high cycle life, fast dynamic response, and ability to operate at higher temperatures. Typically, they provide a high specific power density and low specific energy density around 1-10 Wh/kg [11]. Due to these salient features, they are primarily used in pulsed power applications such as electric transit buses [12], railway traction systems [13], grid-connected systems [14], electrified aircraft [15], hybrid excavators [16], and electric ships [17]. Furthermore, the fast charging capability and less maintenance of SCs enable them to use in renewable energy systems such as solar [18], FCs [19], and wind energy harvesting applications [20]. However, SC banks in such applications are subjected to a wide terminal voltage variation during the charge and discharge process. Therefore, a power converter is interfaced with an SC bank to stabilize the output voltage suitable for the loads.

In Contrast to the Li-ion batteries, the charge and discharge behavior of SCs are linear in nature. The charge/discharge characteristics of an SC is shown in Figure 1.4.

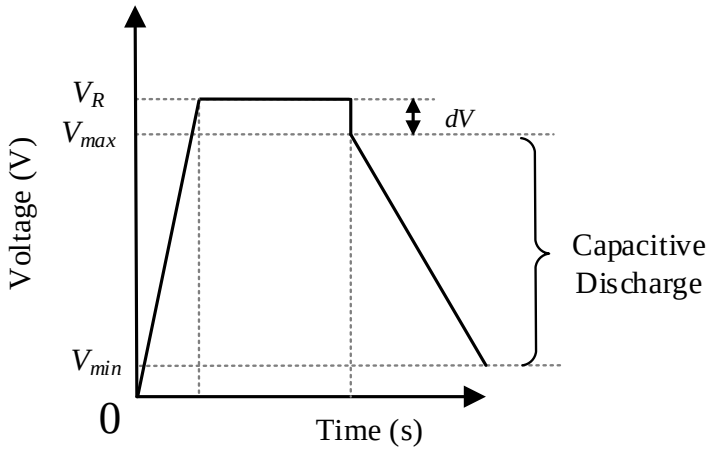

Figure 1.4. Charge and discharge characteristics of an SC.

The SC is charged until the terminal voltage reaches its maximum rated voltage (V_R). When the power source is disconnected, the terminal voltage drops by dV due to its internal ESR [21]. On the other hand, the SC voltage falls from the V_{max} to V_{min} during discharge. The characteristics and performance comparison of the widely used Li-ion batteries and SCs are presented in Table 1.1.

Table 1.1. Comparison between Li-ion batteries and SCs

Function	Li-ion battery	Supercapacitor
Specific Energy (Wh/kg)	230	1-10
Specific Power (kW/kg)	2.5	Up to 10
Cycle life	<5000	>500,000
Operating Temperature (°C)	-20 to 60	-40 to 65
Cost per Wh ($)	2	20

1.2.3. Battery-Supercapacitor Hybrid

An EV with the battery only ESS operating in the urban driving pattern results in demanding transient power. As a result, the batteries are forced to operate at high discharge rates in shorter periods. This issue is tackled by employing an oversized battery unit that offers good power densities [22]. Nevertheless, this solution raises the overall weight and cost of the ESS. Thus, batteries are combined with other power sources to deliver the required dynamic power to the load. There is a wide variety of power units that are used to handle transient load power such as, pumped hydro, flywheel energy storage, and SCs [23]. These are used in conjunction with batteries to form an effective HESS for different applications. The design of HESS should offer high specific energy density, high specific power density, less maintenance at lower system costs.

From the Ragone plot of various storage elements [24], it is observed that SCs offer high power density compared to the other storage elements. Whereas batteries provide high energy density. To drive an electric powertrain at dynamic loads, SCs are the most appropriate device to be selected in conjunction with batteries. A simplified plot for battery-SC hybrid energy storage is shown in Figure 1.5.

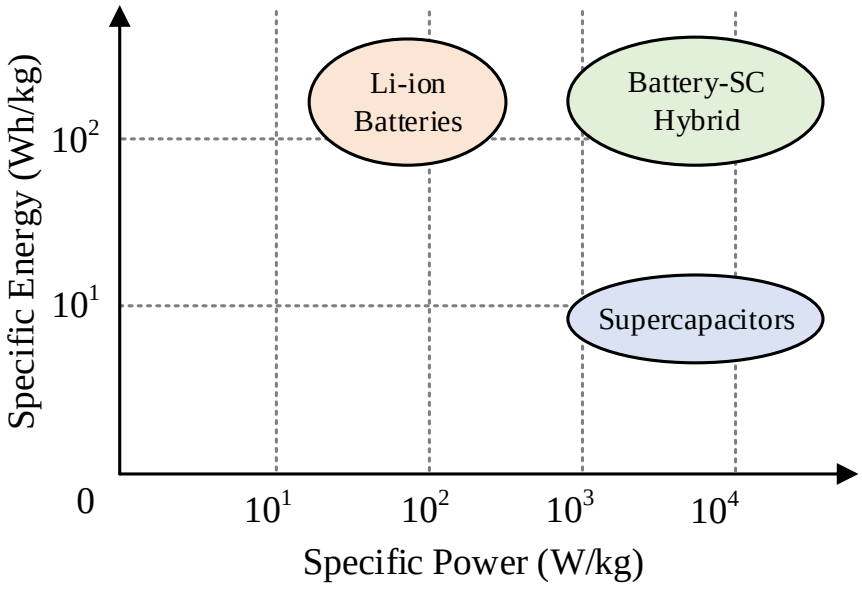

Figure 1.5. Ragone plot of battery-SC hybrid.

A power electronic interface is used to combine batteries and SCs to regulate a constant dc-link voltage. Various dc-dc power converter interfaces were available to merge two energy sources [57] and are selected based on the application, sizing, and cost. The most efficient approach for the battery-SC hybrid system is using two different dc-dc converters for each energy storage device as shown in Figure 1.6.

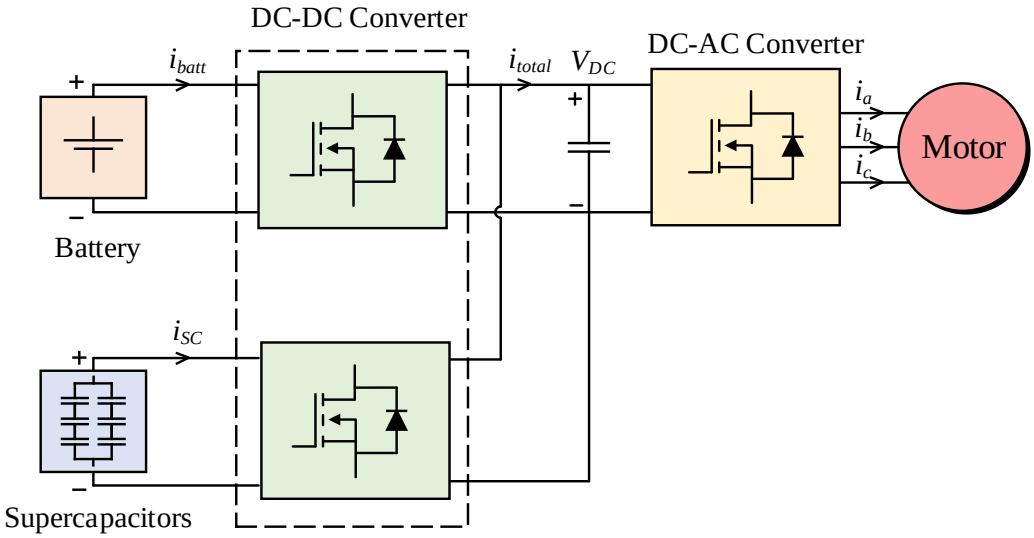

Figure 1.6. HESS-based EV propulsion system.

1.3. Motivation

The key challenge in the EV market is to deliver an efficient and reliable ESS with an enhanced driving range at less maintenance. Thus, most of the EVs use only batteries as their ESS. Nevertheless, they offer less specific power density and cannot be discharged and charged at higher charge rates (C-rates) [25]. In practice, an EV with a battery as a primary source undergoes peaky load demands. To deal with such transient demands, heavy sized batteries are employed. Thus, increases the system weight and costs [26]. In such cases, additional power sources such as SCs can be used in combination with batteries to deliver pulsed power to drive the motor. This HESS enhances the life span of batteries by offering an extended driving range of an EV. Moreover, the overall weight and cost of ESS are significantly reduced. However, this configuration requires a power electronic interface with a proper load power allocation control between two sources. On the other hand, an SC bank delivering high power to the load utilize only 49% to 72% of their energy [27]. To boost their energy delivery efficiency, bank switching topologies can be employed for SCs in HESS.

1.4. Literature Review

The SCs offer a low specific energy density that restricts them from delivering their full energy to the high-power loads. As discussed, the energy utilization efficiency of an SC during discharge is relatively low. Moreover, SCs are typically rated at lower voltage levels and are connected in series combinations to form a bank with minimal capacitance. As a result, SCs in HESS provides the least power delivery duration. In order to serve a continuous series of transient load demands, the bank is required to be recharged either from batteries or regenerative power. As a consequence, the burden on batteries gets increased which is subjected to charge the SC bank and driving the propulsion system simultaneously. Therefore, appropriate power management of SC bank is required to enhance their cell energy utilization and power delivery duration in HESS. Furthermore, the SC bank in HESS results in higher voltage variations at the SC bank terminals which raises the current stress on the active and passive devices of the bidirectional dc-dc converter and diminishes its conversion efficiency.

1.4.1. Previous Work

In recent years, several techniques and control schemes are presented to obtain maximum energy from SCs with an extended power discharge time. Among them, bank-switching techniques are well-addressed approaches to achieve the aforementioned characteristics [28]-[33]. A simple series-parallel changeover circuit is presented in [28] to improve the energy utilization of SCs during discharge. However, this topology offers two-level switching that is not effective in minimizing the terminal voltage fluctuations. To enhance the SC cell energy utilization by addressing the voltage variations, three-level switching circuits are implemented [32], [33]. Nevertheless, these techniques require an intricate power management scheme. Moreover, the switch count and its control complexity are increased with an increase in the sizing level of the bank. Indeed, none of these topologies are verified on real-time applications such as EVs and railway traction systems. In this context, no studies related to the bank switching methods in terms of power delivery time and discharge energy utilization of SCs in HESS-based EVs are conducted. Therefore, it is highly essential to investigate the voltage variations, SoC, and DoD in an SC bank under real-time driving scenarios.

1.5. Thesis Objectives

Addressing the aforementioned concerns, the main purpose of this work is to design and implement a simple bank switching architecture for SCs to enhance their cell discharge energy utilization, power delivery duration with controlled voltage variations in HESS. In accordance with this aim, some of the most important objectives of this work are,

1. To implement a simple bank switching configuration and control of an SC bank to enhance its discharge energy utilization with increased power delivery duration.
2. To verify the impact of the SC bank switching on the passive devices of the bidirectional dc-dc power converter.
3. To implement and analyze the key performance of the SC bank switching circuit in battery-SC based HESS application.
4. To conduct a real-time case study on an EV under various standard drive cycles and verify the SC bank in terms of voltage variation, SoC, and DoD.

1.5.1. Organization of Thesis

The thesis is arranged as follows,

- Chapter 2: This chapter describes the internal construction of SCs and their electrical characteristics. The charge and discharge behaviors are analyzed in detail. Besides, the minimum discharge voltage analysis is conducted which is essential to examine the energy utilization efficiency of an SC.
- Chapter 3: The proposed bank switching architecture and a three-level control for SCs are discussed. A design methodology to size the proposed SC bank switching for various loads is presented. The charge and discharge behavior of an SC bank with the switching circuit is detailed. A comparative analysis during discharge is performed with the non-switched SC bank and a conventional bank switching approaches.
- Chapter 4: A bidirectional dc-dc converter is designed with closed-loop PI control and is associated with the proposed SC bank. The impact of bank switching on the inductor is analyzed by acquiring inductor current variations during the discharge operation.
- Chapter 5: This chapter employs the battery in conjunction with the proposed SC bank to form the HESS. The control algorithm for the load power allocation and bank switching is implemented for an EV. A detailed case study is conducted for the four standard driving schedules.
- Chapter 6: This chapter sums up the major points and outlined with contributions, conclusions, and future work.

Chapter 2

Supercapacitors

This chapter explains the fundamentals of SCs and their electrical characteristics that include construction, charge/discharge behavior. The importance of SC cell voltage balancing is discussed. In the final section of this chapter, detailed simulations and experimental studies of SC banks for constant voltage charging and constant resistive discharging are presented.

2.1. Construction of Supercapacitors

SCs are also termed as EDLCs or ultracapacitors due to the formation of a dual-layer on the separator interface. Typically, the internal structure of an SC comprises two porous carbon electrodes and a separator between them as shown in Figure 2.1. The surface area of carbon is high and offers a near-ideal charge/discharge characteristics [34]. The electrodes are actively excited and increase the diameter of pores on their surface. As a result, the carbon electrodes absorb more ions and offer high capacitance per unit.

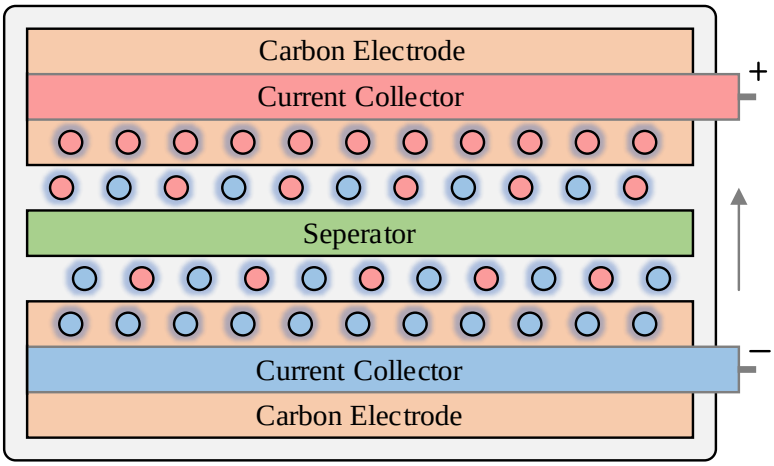

Figure 2.1. The internal construction of an SC.

An aqueous or non-aqueous electrolyte is employed in SCs that flows between the electrodes through the separator layer. The smaller the thickness of separator, the higher the capacitance. The energy densities of the aqueous and non-aqueous electrolytes are around 5500 Wh/m^3 and 20,000 Wh/m^3 respectively [35]. Usually, non-aqueous electrolyte offers high operating voltages with high ESR. Whereas the aqueous electrolyte provides low voltages with lower ESR. Thus, there is always a trade-off between the ESR and the operating voltages of SCs. For instance, the decomposition voltage of the sulphuric acid (aqueous) as an electrolyte offers 1.2 V.

Nevertheless, the design of an SC with high operating voltage results in dissociation of its internal carbon electrodes. As a result, the cell is weakened and cannot be used for long term usage. Moreover, the ESR of an SC is also limited to attain high charge and

discharge efficiency. Therefore, the SCs are designed with aqueous electrolytes that offer minimal ESR values with lower operating voltages.

2.1.1. Temperature Dependence

An efficient SC offers high capacitance with lower ESR values. However, these are generally varied and highly affected by their operating temperatures. The SCs with an aqueous electrolyte offers lower ESR and higher capacitance. The viscosity of electrolyte changes at the extreme lower and higher temperatures. As a result, the ionic resistance of ESR is highly affected. Besides, the ions in SCs move rapidly, and outcomes the higher the number of ions at the electrodes. Thus, the self-discharge rate of SCs is significantly increased [36]. The variation of ESR and capacitance of an SC concerning the change of proportion at 25°C is shown in Figure 2.2.

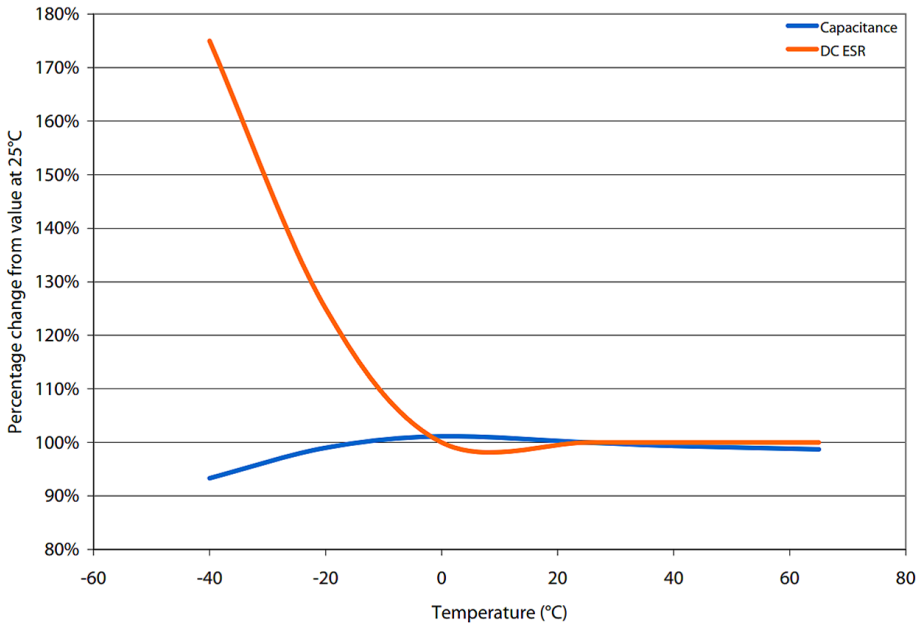

Figure 2.2. Temperature dependency of SCs [37].

2.2. Electrical Characteristics

The electrical behavior of SCs is mostly comparable to the electrolytic capacitors. As discussed in previous sections, the parameters of SCs typically varies with operating temperatures. To analyze the dynamic behavior and performance of an SC, an electrical model is developed.

2.2.1. Equivalent Circuit Model

In practice, the SC possesses varying self-discharge rates, leakage currents, and internal resistance which is responsible for their dynamic behaviors. Moreover, the chemical structure of SCs comprises a stack of carbon electrodes that forms an exceptionally small series inductance which is responsible for the fast pulse change time. Addressing these parameters, the first-order dynamic model presented in [38] is considered for the analysis. The model comprises an R-C parallel circuit with a series resistance (R_{ESR}) as shown in Figure 2.3.

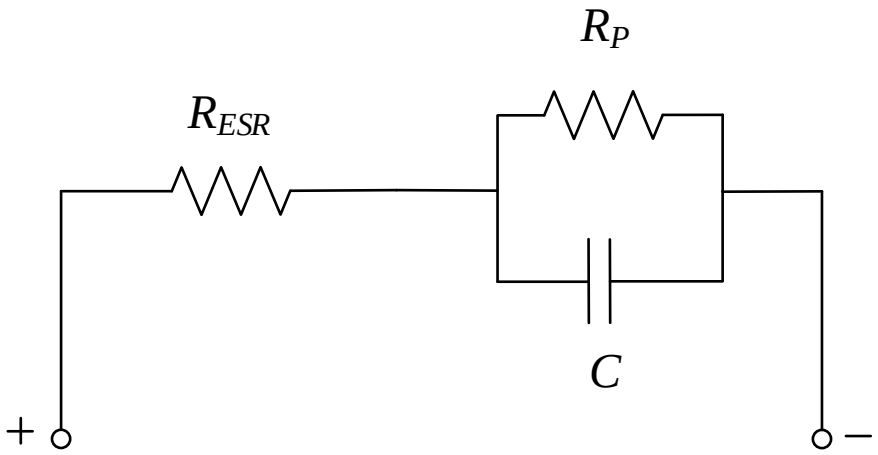

Figure 2.3. First-order equivalent circuit model of an SC.

The capacitor (C) is the overall capacitance of an SC and the resistor R_{ESR} is an internal ESR of SC that is responsible for the losses during charge and discharge operations. The parallel resistor (R_P) accounts for the self-discharge rates that vary during the rapid changes in load demands.

2.2.2. Electrical Parameters

In similar to electrolytic capacitors, the total rated capacitance (C) of an SC cell is given as (2.1). Where ε_r is the relative permittivity, d is the distance between two plates and A is the surface area of SC.

$$C = \frac{\varepsilon_r * A}{d} \tag{2.1}$$

The parameters to measure the total energy and its overall utilization efficiency during charge and discharge is presented as follows,

1. *SC Energy:*

   The total energy of an SC (E_{SC}) is calculated using the following equation (2.2). Where C is the total capacitance and V_R is the rated voltage of an SC.

$$E_{SC} = \frac{1}{2} C {V_R}^2 \tag{2.2}$$

2. *Energy Utilization Efficiency:*

   The specific energy of an SC is varied with the rated voltage. An SC with initial energy (E_i) before discharge is different from the final energy (E_f) after the discharge operation and is highly dependant on its corresponding voltage. The total energy utilization efficiency of an SC during discharge is given by,

$$\eta_{SC} = \left(\frac{E_i - E_f}{E_i}\right) * 100 \tag{2.3}$$

   Where, $E_i = \frac{1}{2} C {V_i}^2$, and $E_f = \frac{1}{2} C {V_f}^2$

3. *State of Charge:*

   The total SoC of an SC is a function of its total electric charge (Q_T) which is obtained from integrating the current (i_{sc}). Typically, the initial charge (Q_i) of a fully charged SC is 100% and a fully discharged SC is 0% [39]. The overall SoC of an SC is given by,

$$SoC = \frac{Q_i - \int_0^t i(\tau) d\tau}{Q_T} * 100 \tag{2.4}$$

$$\text{Where, } Q_T = C * V_T \tag{2.5}$$

   From the above equation (2.5), C represents the total capacitance and V_T is the terminal voltage of an SC. The block diagram of an SC model to obtain the SoC is shown in Figure 2.4.

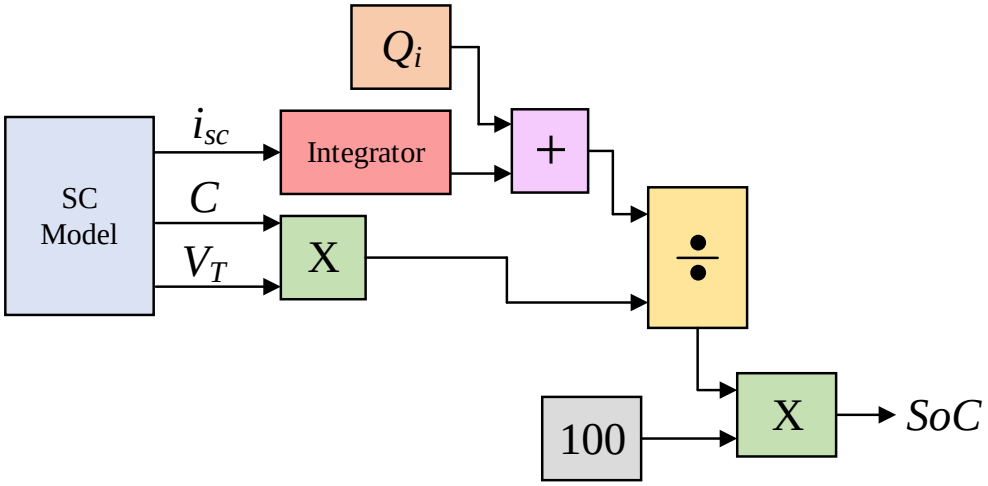

Figure 2.4. Block diagram for SoC identification.

2.3. Charge and Discharge Characteristics

In order to develop an SC bank and realize its operation, it is essential to analyze the charge and discharge behavior of SCs. The SC bank in this work is charged using a constant voltage source and discharged using a constant resistor.

2.3.1. Constant Voltage Charge

A power supply with a constant dc voltage can be used to charge the SC bank. However, this approach results in high inrush currents when connected [40]. Thus, a protective resistor (R_P) is used to limit the charge currents. The schematics of the charging circuit and the V-t characteristics are shown in Figure 2.5(a) and (b) respectively.

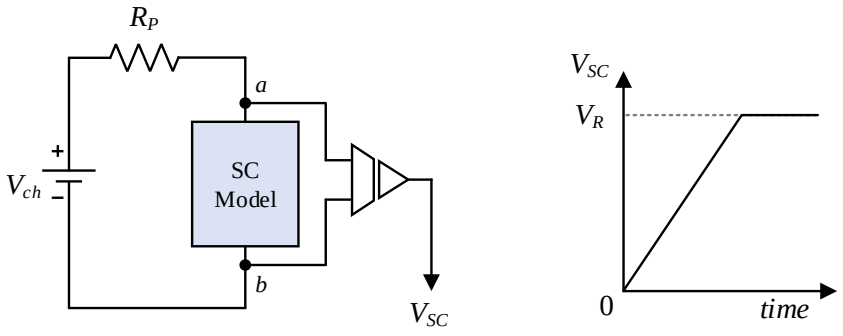

(a) (b)

Figure 2.5. Constant voltage charging (a) circuit and (b) V-t characteristics.

Typically, the considered charge voltage (V_{ch}) should be approximately equal to the maximum rated voltage of an SC bank (V_R),

$$V_{ch} \cong V_R \tag{2.6}$$

The value of R_P for a given charge voltage (V_{ch}) is determined by the maximum charge/discharge current (I_{max}) and ESR which are specified in the manufacturer's datasheet i.e. given by

$$R_P = \frac{V_{ch}}{I_{max}} * ESR \tag{2.7}$$

The total charging time (t_{ch}) of an SC bank with a total capacitance C, rated at V_R given by,

$$t_{ch} = \ln\left(\frac{V_{ch}}{V_{ch} - V_R}\right) * (R_P + ESR) * C \tag{2.8}$$

2.3.2. Constant Resistor Discharge

The SC bank is discharged using a constant resistor at the load (R_{Load}) as shown in Figure. 2.6(a). The terminal voltage of an SC bank (V_{SC}) in this approach falls linearly to the minimum discharge voltage (V_{min}). The total discharge time for a specific load resistance depends on the maximum voltage (V_{max}), and the ESR of the bank and is calculated by [41],

$$t_{disch} = \ln\left(\frac{V_{max}}{V_{min}}\right) * (R_{Load} + ESR) * C \tag{2.9}$$

The V-t characteristics of an SC bank discharged from V_{max} to V_{min} using a constant resistor is shown in Figure 2.6(b).

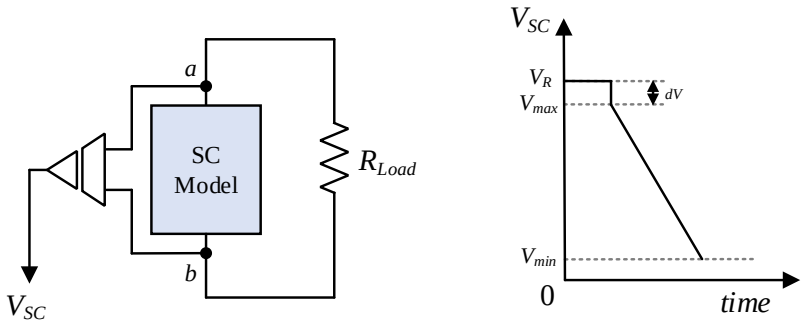

(a) (b)

Figure 2.6. Constant resistive discharging (a) circuit and (b) V-t characteristics.

Moreover, the terminal bank voltage during discharge is dropped from V_R to V_{max} for a difference (dV) which is due to the internal ESR of an SC bank. The higher the ESR, the maximum the voltage drop across the terminals is observed [24]. Therefore, the capacitive discharge region is from V_{max} to V_{min} respectively. The maximum voltage of an SC during discharge after the voltage drop is obtained from,

$$V_{max} = I_{max} * ESR \tag{2.10}$$

2.3.3. Constant Power Discharge

In order to attain the linear discharge characteristics of an SC bank, a constant power source is used for discharge which is obtained by using a power converter as load i.e. shown in Figure 2.7.

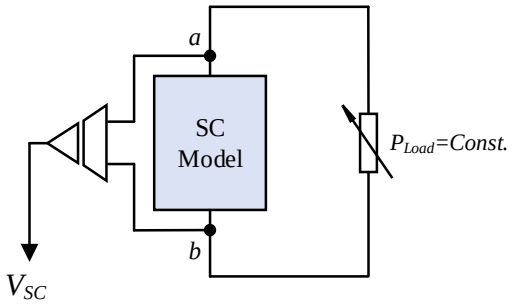

Figure 2.7. Constant power discharging of SC bank.

The discharge time of an SC bank for a constant power load depends on the maximum rated voltage (V_R), and the minimum discharge voltage (V_{min}) i.e. is given by [41],

$$t_{disch} = (V_{max}^2 - V_{min}^2) * \frac{C}{2 * P_{Load}} \tag{2.11}$$

On the other hand, the minimum current allowed to discharge from an SC is calculated by,

$$I_{min} = \frac{P_{Load}}{V_R} \tag{2.12}$$

2.3.4. Minimum Discharge Voltage

Typically, the SCs are discharged from V_{max} to V_{min}, but not till 0 V. A fully discharged SC always hold a small charge with some minimal voltage (V_{min}) that helps them to recharge quickly. Thus, the minimum discharge voltage of as SC for a constant power load (P_{load}) is

determined by the maximum discharge current (I_{max}) which is provided in the manufacturer's datasheet, is given by,

$$V_{min} = \frac{P_{Load}}{I_{max}} \tag{2.13}$$

Consider an SC rated at 50 F, 2.7 V comprising a maximum discharge current (I_{max}) of 33.7 A assumed as a constant for the analysis. The SC is connected to a constant power load and is allowed to discharge from V_{max} to V_{min}. The V_{max} for the SC is 2.1 V i.e. obtained from the equation (2.10). The minimum discharge voltage of an SC (50 F, 2.7 V) for different power loads is shown in Figure 2.8.

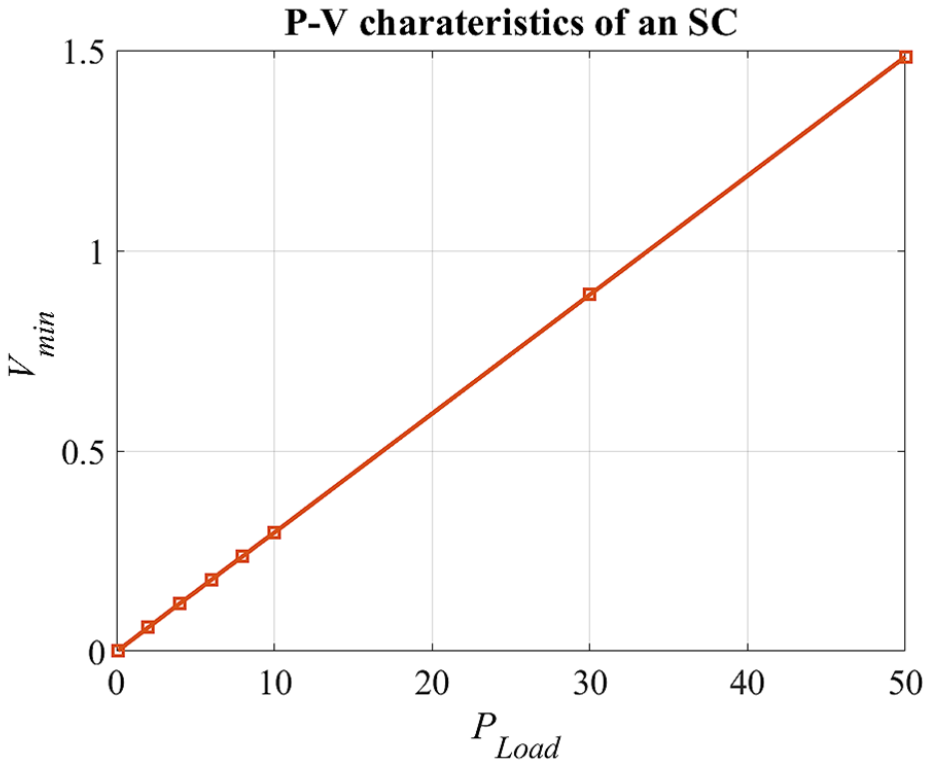

Figure 2.8. P-V characteristics of an SC.

For a 10 W power load, it is observed that the considered SC is discharged from 2.1 V to 0.3 V. Furthermore, the minimum voltage value of an SC rises with the increase of the load power demands. Therefore, the minimum discharge voltage of any SC bank for the high-power applications is restricted to a higher value of the discharge voltages (V_{min}). Moreover, this further affects the energy utilization efficiency of each SC in a bank.

2.4. Voltage Equalization

Generally, SCs are rated at lower voltages i.e. ranging from 1.5 V to 2.7 V which is due to the electrolytic decomposition voltage discussed in the previous sections. Thus, they are connected in series combinations to meet the load voltage requirements. However, each SCs comprises a different tolerance level which results in the voltage difference of individual SC cells during charge and discharge operations. As to avoid an imbalance in individual SC voltages, the voltage balancing circuit is employed in a bank. Several active and passive balancing circuits are available that offer high balancing efficiency with minimal power losses [42]. Among them, a low-cost resistive (passive) balancing circuit is chosen for this work. The schematic of a resistor balancing circuit is shown in Figure 2.9.

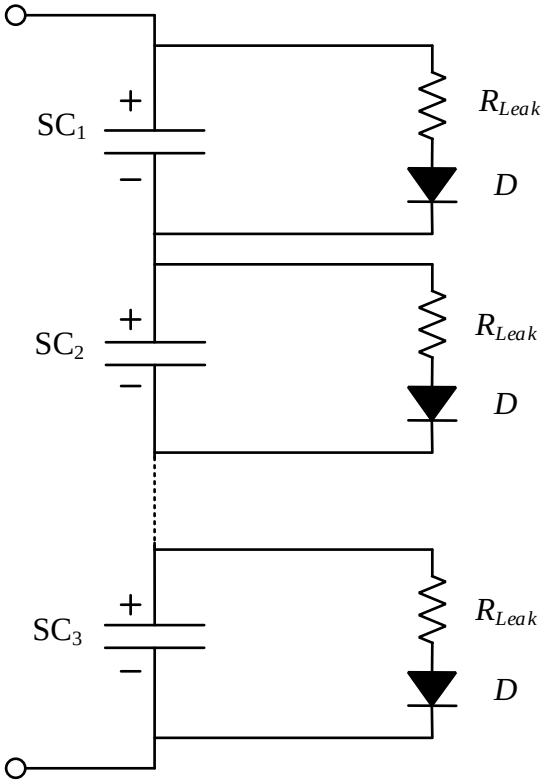

Figure 2.9. Resistive voltage balancing circuit.

A leakage resistor (R_{Leak}) and a diode are connected in parallel with each SC in a bank. The voltage of an SC is higher than the forward voltage drop of diodes. As the voltage of one SC is higher, it is discharged onto the resistor and dissipates its energy as heat.

Nevertheless, a parallel resistor always results in increasing the self-discharge rate of an SC [43]. Thus, this approach is not highly recommended.

The value of R_{Leak} for a specific SC bank is obtained from the following equation,

$$R_{Leak} = \frac{V_R}{I_{Leak}} \tag{2.13}$$

Where, V_R is the maximum rated voltage of an SC bank, and I_{Leak} is the leakage current of individual SC which is obtained from the manufacturer's datasheet.

2.5. Simulations

To analyze the practical behavior of an SC bank, the simulation studies are conducted during the charge and discharge operations. An SC bank rated 400 F, 7.5 V which comprises total energy of 11.2 kJ is considered for the analysis.

2.5.1. Constant Voltage Charge Characteristics

The dc voltage source delivering a constant 20 V is considered and the initial minimum voltage of an SC bank is set to 2.5 V. A protective resistor rated 1 Ω is used. The results of the SC bank during charging is shown in Figure 2.10. The results show that the SC bank takes 134 s to fully charge each SC and the overall bank from 2.5 V to 7.5 V.

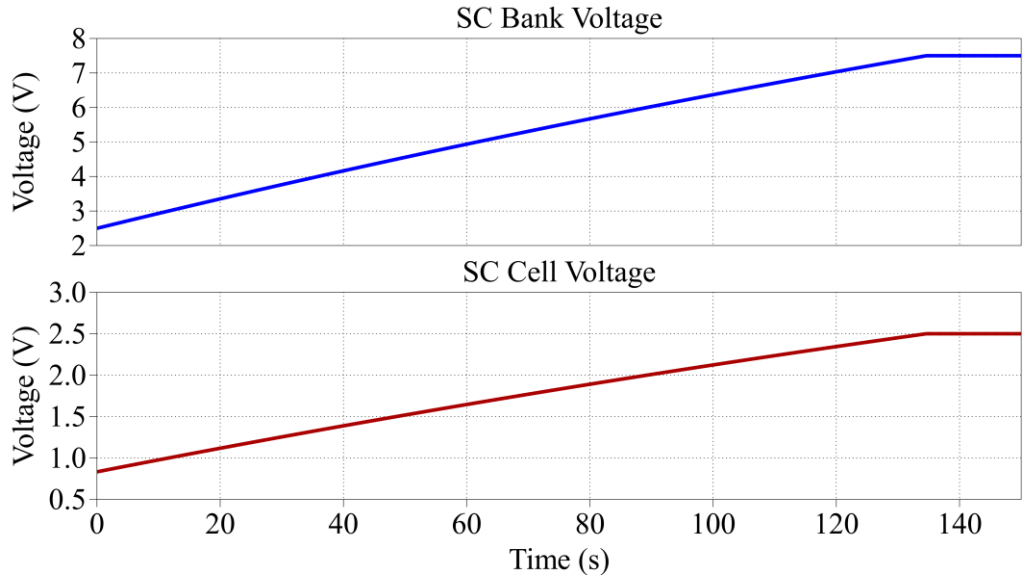

Figure 2.10. Simulation results of SC bank during constant voltage charging.

2.5.2. Constant Resistor Discharge Characteristics

A constant load resistive load rated 0.5 Ω is connected to discharge the SC bank. The maximum and minimum considered voltages (V_{max} & V_{min}) of an SC bank are 7.5 V & 4 V respectively. The simulation results are shown in Figure 2.11.

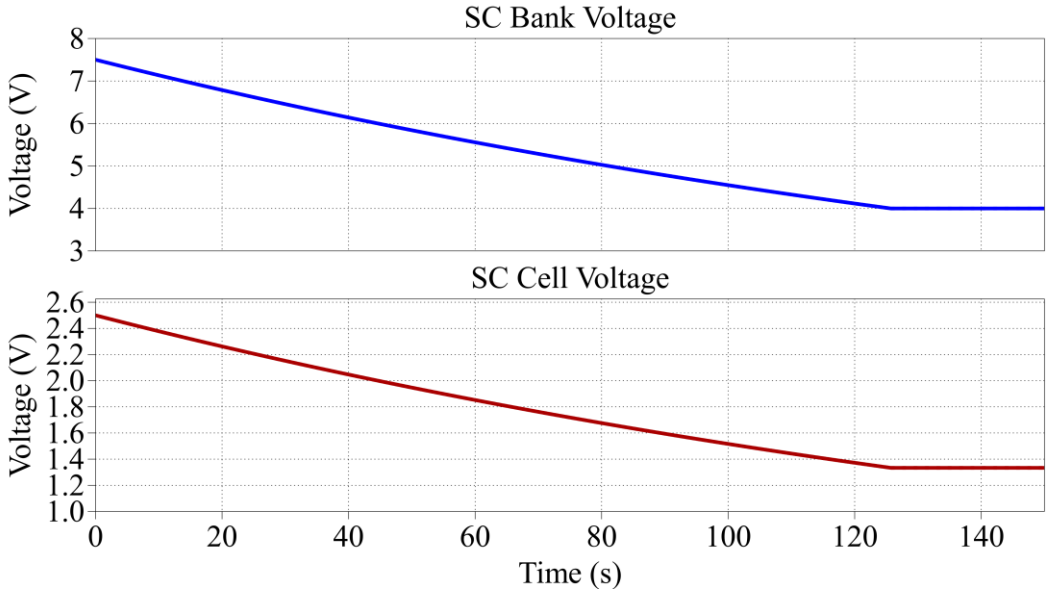

Figure 2.11. Simulation results of SC bank during constant resistor discharging.

2.6. Experimental Validation

In order to verify the practical behavior of SCs, experimental validation is carried out on a laboratory prototype. The SC bank is scaled down for the experiments and rated at 22 F, 8.1 V which has the total energy of 721.7 J. The aforementioned resistive balancing circuit with a resistor (R_{leak}) rated 47 kΩ is used to balance the individual cell voltages in the bank.

2.6.1. Constant Voltage Charge Characteristics

A dc power supply delivering the constant 8.2 V of charge voltage (V_{ch}) is considered for the experiments. The initial voltage of an SC bank is 2.6 V and is allowed to charge till rated voltage (V_R) i.e. 8.1 V. The protective resistor rated 0.5 Ω is connected in series with the power supply. The experimental results for the constant voltage charging are shown in Figure 2.12. The results show that the SC bank voltage is raised from 2.6 V to 8.1 V in 28

s. Whereas the cell voltage of each SC in that bank is increased from 1.2 V to 2.7 V respectively. Thus, the results are similar to the simulations.

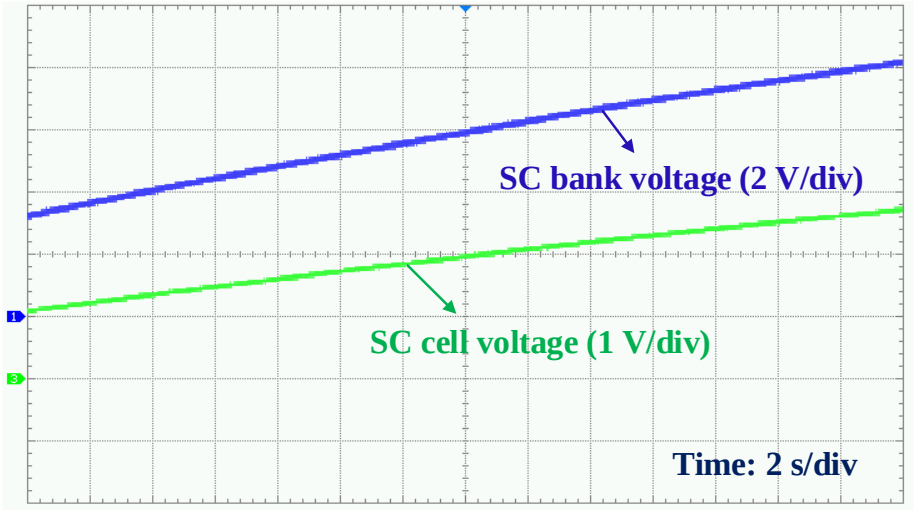

Figure 2.12. Experimental results of SC bank during constant voltage charging.

2.6.2. Constant Resistive Discharge Characteristics

Due to the internal ESR of an SC bank, the maximum voltage of an SC bank is calculated from (2.10) which is dropped from 8.1 V to 7.6 V. Thus, the maximum and minimum rated voltages of SCs are 7.6 V and 4 V respectively which is similar to the simulation results (discharge). A constant resistor rated 1 Ω is used to discharge the bank. The experimental results during constant resistive discharge are shown in Figure 2.13.

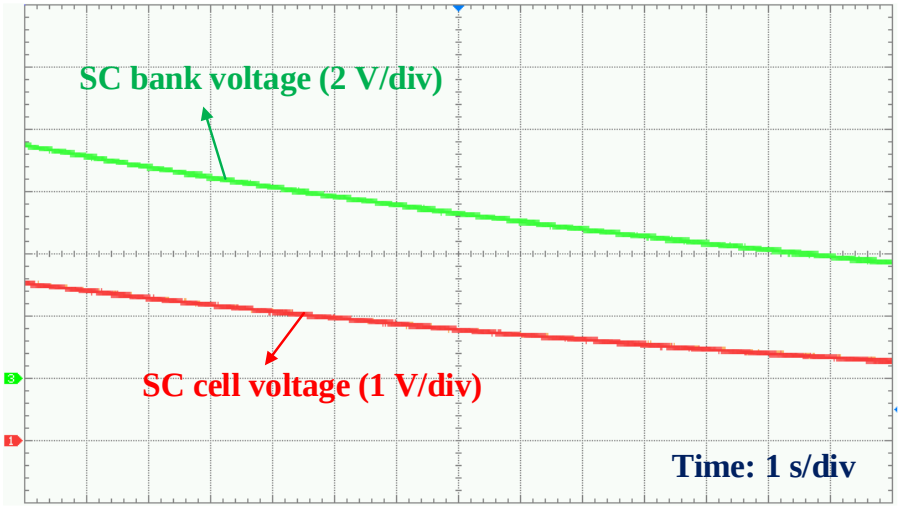

Figure 2.13. Experimental results of SC bank during constant voltage discharging.

It is observed that the SC bank is discharged from 7.6 V to 4 V in 12.5 s. Likewise, the SC cell voltage is dropped from 2.5 V to 1.4 V. Thus, offering 68.6% of cell energy utilization efficiency during discharge.

2.7. Summary

This chapter details the fundamentals of SCs and their electrical characteristics. Moreover, the charge/discharge behavior of SC bank using various approaches that include constant voltage charging, constant resistive discharging, and constant power discharging is studied. The related simulations and experimental validation are conducted for the SC banks. It is noticed that the SC bank can be fast-charged and discharged linearly.

Besides, a detailed analysis of the minimum discharge voltage of SCs is conducted. It is concluded that the minimum voltage of an SC bank highly depends on the maximum discharge currents and the power demand. As a result, the load applications demanding the higher power restricts the SC bank to a higher value of the minimum discharge voltage (V_{min}). This affects the SC cell energy utilization efficiency by restricting the deep discharge of an SC bank. To enhance the cell energy utilization and power delivery duration of an SC bank, a new bank switching concept is proposed in the next chapter.

Chapter 3

Proposed Bank Switching

The previous chapters gave us an insight into the SCs and their concerns in HESS based EV applications. As mentioned, the SC bank deficits in delivering their full energy for higher power loads and lacks in specific energy density. The typical energy utilization efficiency of an SC cell during discharge is nearly limited to 72%. To enhance the power delivery and energy usage of an SC, a new bank switching topology is proposed in this chapter. The fundamentals of SC bank switching and its behavior during charge and discharge operations are detailed. The proposed technique is compared with the conventional bank switching topologies in terms of power delivery duration, SC cell energy utilization, and system efficiency. Furthermore, the power loss of the system due to the switching circuit and the overall system costs are analyzed and discussed in this chapter.

3.1. Bank Switching

In similar to electrolytic capacitors, the bank capacitance of SCs increases when connected in parallel and the bank voltage rises when connected in series combination. As discussed in Chapter 2, the SCs rated at very low voltages ranging from 1.3 V to 2.5 V [44]. Thus, they are connected in series combinations to meet the load voltage requirements and by lacking in energy storage capability. To utilize their full energy, a switching circuit is implemented in the SC bank that makes the transition series-parallel combination of SC cells and maintains the bank terminal voltage within the threshold limits. Such reconfigurable SC bank is further connected to a dc-dc power converter that accepts the varying voltages and delivers the constant dc-link voltages at the outputs. This is a simple and effective solution to enhance the energy utilization of the SC cell in a bank during the discharge operation. Moreover, this technique is employed in electric vehicular applications in which the SC bank can deal with shorter transient power demands using a subsequent switching mechanism [45].

3.1.1. Series-Parallel Bank Switching

Typically, the energy utilization efficiency (η_{SC}) of SCs is inversely proportional to the sizing of the SCs in a bank. The smaller the capacitance results in higher energy utilization efficiency and vice versa. Contemplating this principle, a simple two-level bank switching technique is presented in [28]. The bank comprises three switches that reconfigure the SC's to series and parallel combination with respect to the charge and discharge operations as shown in Figure 3.1.

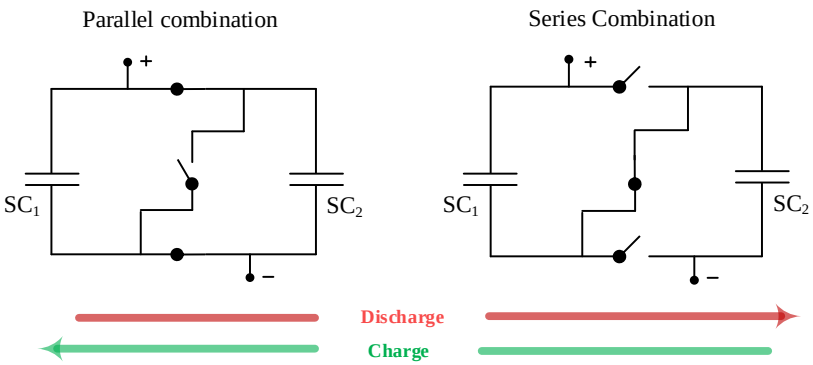

Figure 3.1. Series-parallel change-over circuit.

Initially, all SCs in the bank are charged to its rated voltage. The SC bank in parallel combination with high capacitance is allowed to discharge using a constant resistive load. When the terminal voltage of the bank reaches a pre-set lower threshold point, all SCs in the bank are reconfigured into the series combination that reverts the bank voltage to its maximum rated voltage with lower capacitance. Therefore, the series-parallel changeover technique results in achieving a significant rise in SC cell energy utilization efficiency by 20%. As the sizing level of an SC bank increases, the two-level switching circuit cannot handle higher current stress. Thus, several three-level switching circuits are presented in the literature [32], [33] discussed in Chapter 1. Nevertheless, these configurations result in higher switch count with an intricate control that increases the overall system complexity and costs.

3.2. Auxiliary Bank Switching

To simplify the complex three-level bank switching circuits with an enhanced SC cell energy utilization efficiency, a new SC bank switching architecture is proposed and termed as "Auxiliary bank switching" as shown in Figure 3.2.

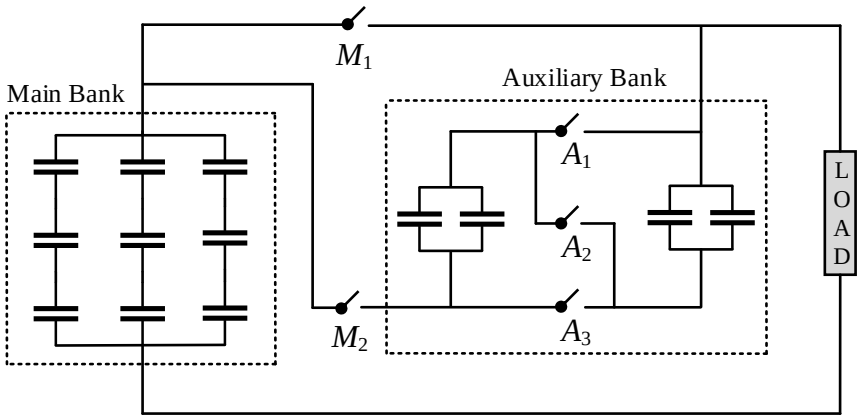

Figure 3.2. Proposed auxiliary bank switching architecture.

The proposed configuration comprises two individual sub-banks namely the main bank and the auxiliary bank. The main bank has a stack of SCs connected in series combination to meet the load voltage requirements without any switching circuit. On the other hand, the auxiliary bank consists of an aforementioned series-parallel switching circuit with the switches A_1, A_2, and A_3. The auxiliary bank is re-configured between series and parallel

modes and connects to the main bank using the switches M_1 and M_2 with respect to the varying load demands.

3.2.1. Modes of Operation

The modes of operation for the proposed architecture during discharge mode are shown in Figure 3.3. To deliver the transient power to the load, the main bank is connected/disconnected to the auxiliary bank using the switches S_1, S_2. On the other hand, the auxiliary bank with a series-parallel change-over circuit uses the switches S_3, S_4, S_5, and S_6 respectively. To suppress the inrush currents due to switching of SCs in the auxiliary bank, a bidirectional switch for A_1 is considered which provides an automatic current distribution when changed from parallel to series combination during charging.

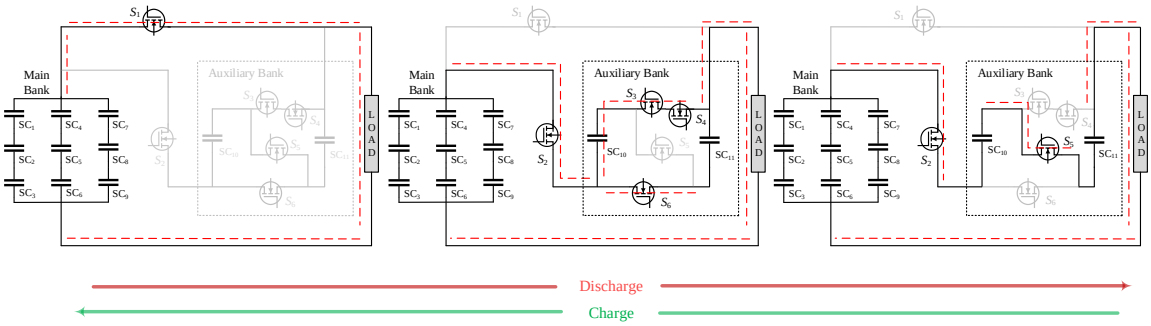

(a) (b) (c)

Figure 3.3. Modes of operation of the proposed architecture: (a) Main bank alone, (b) Main bank and auxiliary bank (parallel), and (c) Main bank and auxiliary bank (series).

At first, all the SCs in the bank are charged to its rated voltage. The SCs in the auxiliary bank are initially connected in parallel combination and is switched to series mode as per the load requirement. A constant resistive load is used to analyze the current flow of the circuit in each mode which is represented in the red dotted line. The proposed circuit is operated as follows,

1. *Main bank alone mode:* In level 1, only the main bank is used to deliver the power required by the load i.e. switch S_1 is turned ON, and S_2, S_3, S_4, S_5, S_6 are in OFF condition as shown in Figure 3.3(a).
2. *Main bank and auxiliary bank (parallel) mode:* When the main bank voltage drops to the first pre-set threshold (V_{Th1}), The auxiliary bank (parallel) is connected to the main

bank in series combination by turning ON the switches S_2, S_3, S_4, and S_6. Whereas the other switches S_1, and S_5 are in OFF state as shown in Figure 3.3(b).

3. *Main bank and auxiliary bank (series) mode:* In level 3, the auxiliary bank voltage is continuously monitored. When the total SC bank voltage falls to the second pre-set threshold (V_{Th2}), the SCs of the auxiliary bank are switched from parallel to the series mode to increase the total SC bank voltage i.e. the switches S_2 and S_5 are turned ON and S_1, S_3, S_4, S_6 are in OFF condition as shown in Figure 3.3(c).

Thus, all the SCs in the bank are discharged to its minimum rated voltage. The switching sequence of the proposed architecture is presented in Table 3.1.

Table 3.1: Switching Sequence for proposed bank switching

Switching level	Conducting Switches
1	S_1
2	S_2, S_3, S_4, S_6
3	S_2, S_5

Similarly, the modes of operation of the proposed architecture during charge are vice-versa, i.e. the modes are operated from level 3, level 2, and level 1 respectively.

3.2.2. Three-level Switching Control

The simple switching control for the abovementioned bank switching method is presented as shown in Figure 3.4. As discussed, the control scheme comprises of three levels of SC bank transitions during charge and discharge mode of operations. The switching between each level is performed by monitoring the main and auxiliary bank voltages (V_{main} & V_{aux}) which are varied as per the load demands.

The first level has no switching circuitry. Thus, the main bank voltage (V_{main}) is monitored continuously. If its terminal voltage is lesser than the first switching threshold value (V_{Th1}), the auxiliary bank in parallel form is connected to the main bank in level 2 to deliver the additional power to the load. Further, the auxiliary bank voltage (V_{aux}) is monitored. In level 3 transition, if the auxiliary bank voltage drops to the second switching voltage threshold (V_{Th2}), the auxiliary SC stack is reconfigured from parallel to series

combination by maintaining the total bank voltage at the nominal level offering the maximum power delivery time. Likewise, the charge mode control flow is performed by reverting the same levels from 3 to 1 respectively.

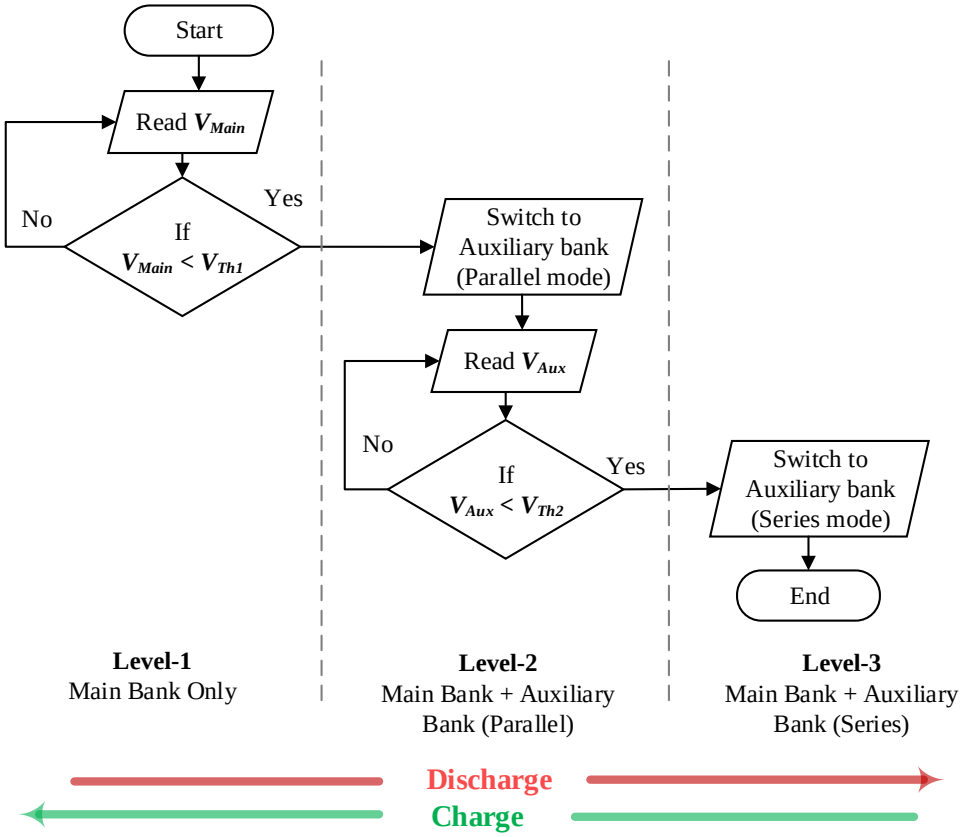

Figure 3.4. Switching control for the proposed bank switching architecture.

3.2.3. Design and Sizing Considerations

The sizing of the proposed SC bank architecture for a specific load is achieved by performing the following design steps:

1. *Voltage Ratings:*

   In level 1 of the auxiliary bank switching method, the main bank alone is used to serve the power demands. Thus, the SCs in the main bank are connected in a series combination to meet the load voltage requirements.

$$V_{main} = V_{load} \tag{3.1}$$

On the other hand, a detailed voltage variation analysis is performed to obtain high SC energy utilization. Various values of voltage variation (ΔV) are considered. The curve of energy utilization concerning voltage variation is shown in Figure 3.5(a). The maximum efficiency is obtained at 36% and 50%. As the higher voltage variations are a concern to the power converter, the smaller value is considered and given as,

$$V_{aux} \cong 0.36 * (V_{main}) \tag{3.2}$$

2. *Capacitance Rating:*

The ideal capacitances of the main and auxiliary banks are acquired from the peak power delivery time of the proposed SC bank. To obtain the maximum power delivery duration, the possible combinations of main and auxiliary bank capacitances that can hold 11.2 kJ of energy are considered. A detailed analysis is carried out by varying the ratio of auxiliary bank capacitance to the main bank capacitance from 0 to 9. It is noticed that the peak point of power delivery time is acquired at a ratio of three as shown in Figure 3.5(b). Hence, the ideal sizing equation of the main and auxiliary banks in the proposed architecture is derived as,

$$C_{aux} = 3 * C_{main} \tag{3.3}$$

The auxiliary bank comprises of SCs in parallel combination. Each branch is sized to the half of the auxiliary bank capacitance and is given by,

$$Branch\ 1 = Branch\ 2 = \frac{C_{aux}}{2} \tag{3.4}$$

3. *Switching thresholds:*

The proposed approach necessitates two switching thresholds to reconfigure the SC bank with respect to the load demands. The first switching threshold is necessitated to connect the auxiliary bank in series with the main bank when the voltage of the main bank reaches a certain threshold point. Though the capacitance of the bank is decreased, the auxiliary bank (parallel) rated with 36% of the main bank voltage is added to the overall bank voltage. Hence, the first switching voltage threshold (V_{th1}) is derived by subtracting auxiliary bank voltage from the main bank voltage i.e.,

$$V_{th1} = V_{main} - V_{aux} \tag{3.5}$$

Secondly, the auxiliary bank is switched from the parallel from to the series from when its corresponding voltage drops to 74%. Thus, the second threshold (V_{th2}) is set as,

$$V_{th2} = 0.74 * (V_{aux}) \tag{3.6}$$

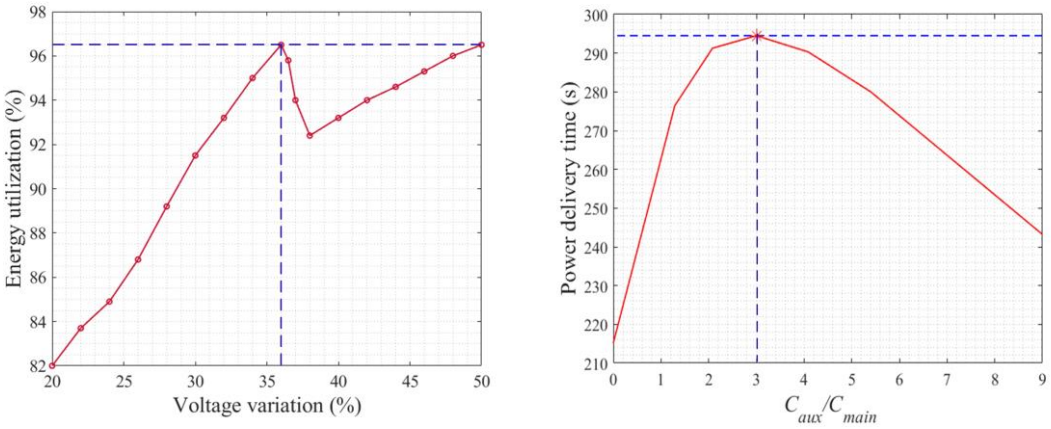

(a) (b)

Figure 3.5. (a) Voltage variation curve and (b) Maximum power delivery time.

4. *Energy Matching:*

The proposed SC bank with switching is compared with the non-switched SC bank by equating their energy. The total energy of an SC bank without switching (E_{SC}) should be equal to the sum of energy of the main bank (E_{main}) and auxiliary bank (E_{aux}).

$$E_{SC} = E_{main} + E_{aux} \tag{3.7}$$

To verify the above equation, a non-switched SC bank rated 400 F, 7.5 V is considered for the analysis. The energy stored in the SC bank without any switching (E_{SC}) is 11.2 kJ. On the other hand, the main bank of the proposed architecture is rated 300 F, 7.5 V with an energy of 8.4 kJ is considered. Assuming the main bank capacitance as a constant, the auxiliary bank capacitance is varied from 0 F to 1500 F. The total energy of main and auxiliary banks acquires 11.2 kJ when at the auxiliary bank with a capacitance at 900 F.

3.3. Simulation and Analysis

The simulation studies of the proposed configuration with a three-level switching control scheme are conducted in the PLECS software platform and validated the same on a developed SC bank prototype. To verify the effectiveness of the auxiliary bank switching configuration, the final results are compared with a non-switched SC bank and a conventional bank switching approach presented in [33].

The SC bank with a total of 11 SCs is considered for the analysis. Nine of them are arranged in the main bank (7.5 V, 300 F) and the rest of them are placed in the auxiliary bank (2.5 V, 900 F). The proposed bank is sized in compliance with the aforementioned design considerations. On the other hand, the non-switched SC bank and the conventional SC bank with the same energy (11.2 kJ) of the proposed SC stack are taken into account to perform the comparative analysis. The proposed power management control is implemented to switch the SC bank as per the monitored voltages (V_{main} & V_{aux}).

3.3.1. Charge Characteristics

The simulation results of the proposed SC bank during the charge operation are performed in the PLECS software platform. The considered minimum bank voltage for the analysis is 2.6 V, and it is allowed to charge to its maximum rated voltage i.e. 7.5 V. A constant dc-voltage source of 20 V is used to recharge the SC bank. A protective resistor rated 1 Ω is connected in series with the power supply to limit the charge currents. The results of the proposed bank switching architecture are shown in Figure 3.6.

Initially, the control and modes of operation for the charging procedure begin by charging the SC cells in the auxiliary bank (series). When the auxiliary bank voltage reaches a pre-set threshold, the SCs in the auxiliary bank are reconfigured from series to parallel combination and recharges them to its maximum voltage. Lastly, the auxiliary bank is disconnected from the main bank and allows only the main SC stack to charge to its maximum rated voltage. The results show that the SCs in the auxiliary bank are charged first and then disconnected from the main bank when it reaches the rated voltage i.e. 2.5 V. On the other hand, the total SC bank voltage is charged to its maximum voltage i.e. 7.5 V.

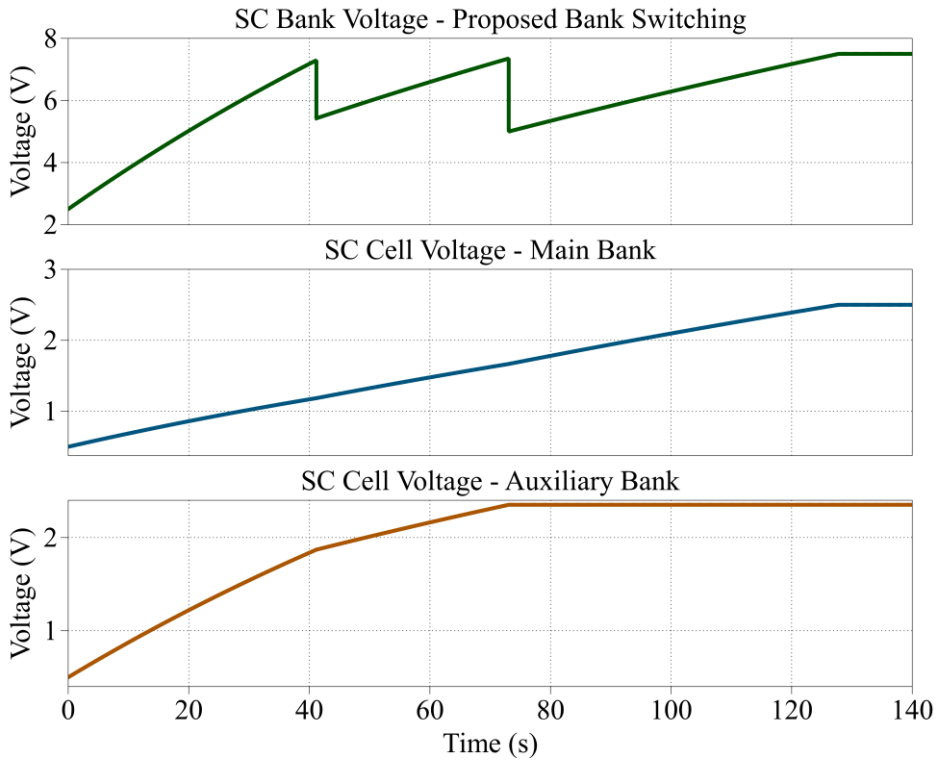

Figure 3.6. Simulation results of the proposed SC bank during charging.

3.3.2. Discharge Characteristics

The SC bank in pulsed power applications mostly operates in small charge-discharge cycles. Thus, the considered maximum and minimum voltages of the bank for this study are 7.5 V and 4 V respectively. A constant resistive load of 0.5 Ω is used to discharge the SC bank. The PLECS simulation results of the proposed configuration in terms of power delivery duration and SC cell energy utilization during discharge are shown in Figure 3.7(a) and (b) respectively.

During discharge, it is observed that the SC bank with a conventional bank switching approach offers a 12% increase in the power delivery time compared to the bank without any switching. On the other hand, the proposed method provides a 15% increase in their power delivery duration as shown in Figure 3.7(a). Furthermore, the cell voltage in the SC bank with a conventional bank switching concept is discharged from 2.5 V to 0.7 V and has 92% of SC energy utilization efficiency, calculated from the equations (2.2), (2.3) discussed in Chapter 2.

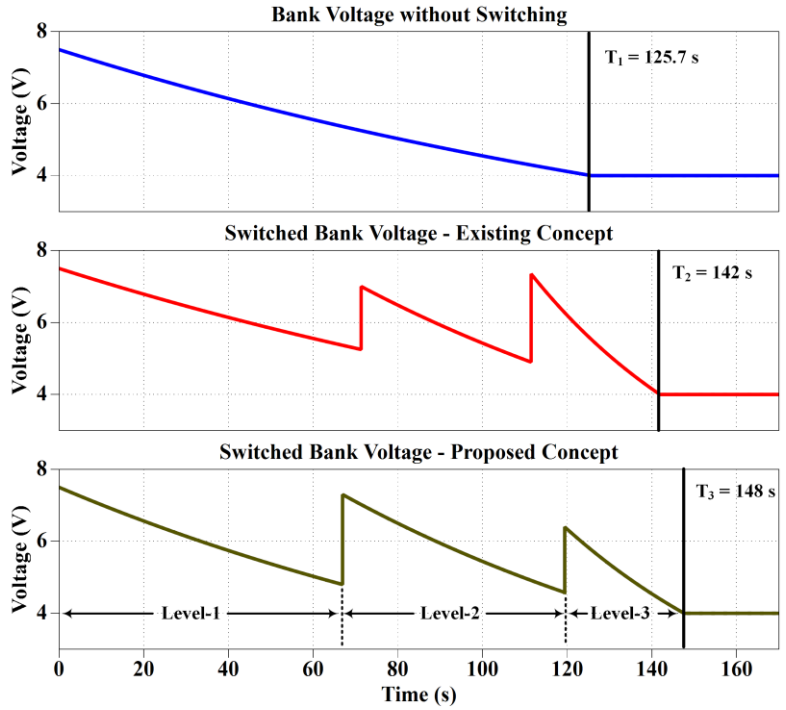

(a)

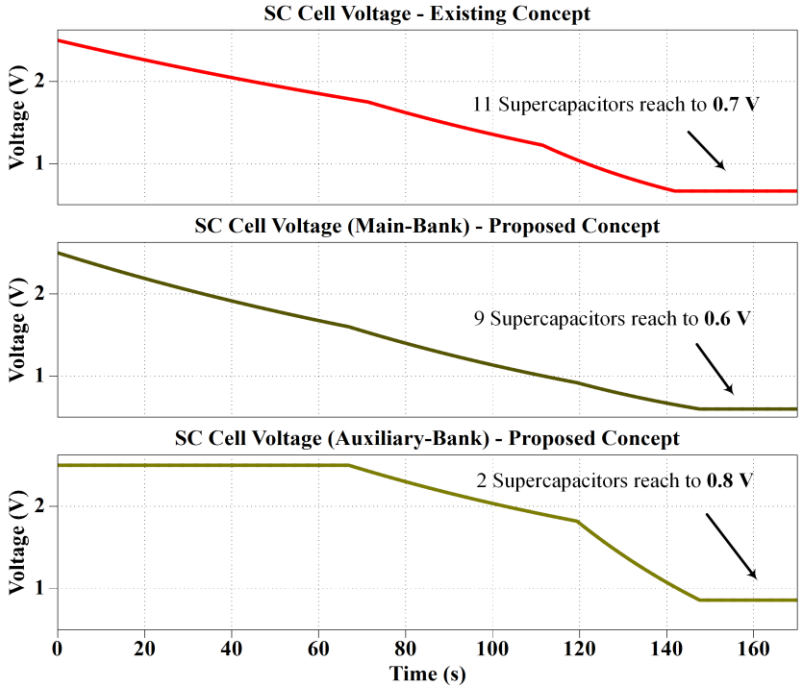

(b)

Figure 3.7. Simulation results of the proposed SC bank during discharge in terms of (a) Power delivery duration and (b) SC energy utilization.

However, the cell voltage of the SC bank with the proposed bank switching technique drops from 2.5 V to 0.6 V and has 95% of SC cell energy utilization efficiency. Moreover, only two SCs in the auxiliary bank are discharged to 0.8 V. This voltage difference is balanced by a proper bank balancing circuit and helps in providing a backup static charge to the deep discharged (0 V) SC bank during the charge mode of operation.

3.3.3. Bank Efficiency Analysis

To verify the overall efficiency of the proposed SC bank (η_{bank}) under various resistive loads, a comparative analysis with a non-switched SC bank (11.2 kJ) during discharge is carried out. The SCs in a bank is allowed to discharge using various resistive loads ranging from 0.1 Ω to 5 Ω. The results of the overall SC bank efficiency under with and without bank switching circuit is shown in Figure 3.8.

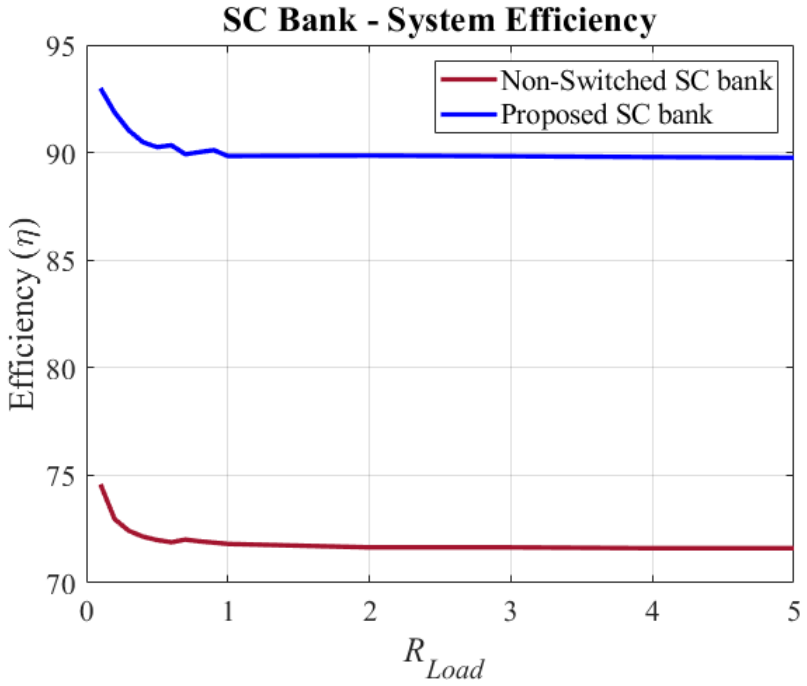

Figure 3.8. SC bank - System efficiency

The plot shows that the system efficiency during discharge of the SC bank under smaller restive loads is high compared to the higher resistive loads. Therefore, the SCs are best suited for the pulsed power applications by delivering higher bursts of currents in shorter periods. Furthermore, the SC bank without any switching provides a 73% average

efficiency. Whereas the SC bank with the proposed switching circuit offers the highest of 92% average system efficiency.

3.3.4. Loss Analysis

Typically, an oversizing of the conventional SC bank switching method outcomes a significant rise in switch count and the voltage ratings of the active MOSFETs. Thus, results in affecting the system efficiency by increasing the switching losses and the conduction losses across the switches. Addressing this issue, a detailed loss analysis for the proposed auxiliary bank switching circuit is performed and compared with the aforesaid conventional bank switching technique. The initial energy of both the SC banks is considered as a constant i.e. 11.2 kJ (3.1 Wh). The thermal model of an active MOSFET (C3M0021120K) is considered for the analysis. The heat sinks are connected to each MOSFET to analyze its switching and the conduction losses. The SC bank is allowed to discharge to a constant resistive load of 0.5 Ω. The results of the current flow through MOSFETs in main and auxiliary banks during the discharge operation are shown in Figure 3.9(a) and (b) respectively. It is noticed that the peak current flowing through the switches associated with the main and auxiliary banks is 15 A. Thus, the MOSFETs are selected with a minimum current rating of nearly greater than 15 A.

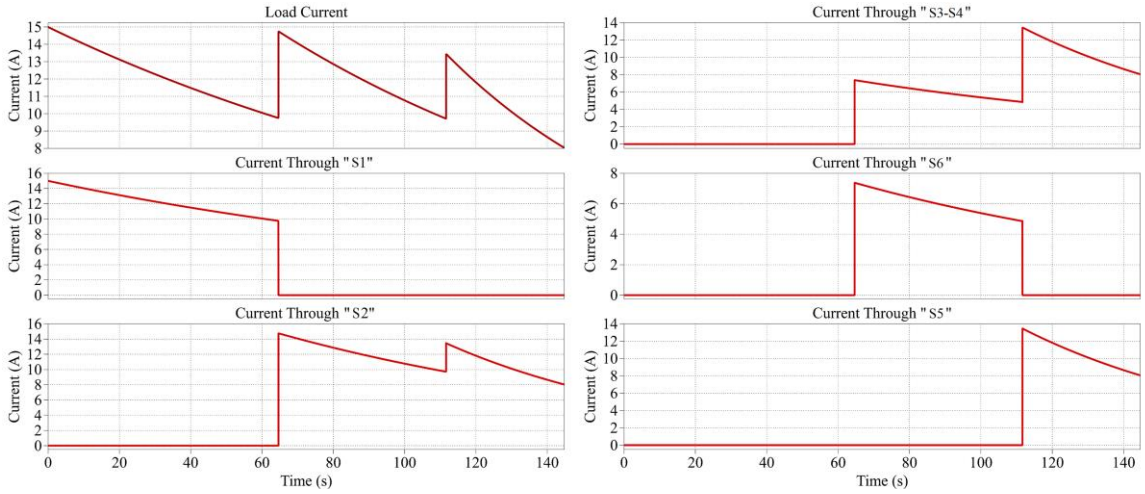

(a) (b)

Figure 3.9. Current stress on MOSFETs in (a) the main bank and (b) auxiliary bank.

Moreover, the mean power loss and the output power of the SC bank are summarized in Table 3.2. The results show that the average power loss due to the switching circuit in conventional bank switching approach results in 15.2 W. Whereas, the mean power loss in the proposed bank-switching circuit offer 7.5 W. Therefore, it is clear that the proposed circuit offer low switching and conduction losses compared to the conventional bank switching topology.

Table 3.2. Evaluation of power loss in the bank switching circuits

Bank switching method	**Mean P_{Loss} (W)**
Without switching	0
Conventional	15.2
Proposed	7.5

The results show that the average power loss due to the switching circuit in conventional bank switching results in 15.2 W. Whereas, the mean power loss in the proposed bank-switching circuit offer 7.5 W. Therefore, it is clear that the proposed circuit offer low switching and conduction losses compared to the conventional bank switching topology.

3.4. Experimental Validation

To validate the efficacy of the proposed switching configuration, the experimental studies are conducted on a laboratory-developed prototype. The overall block diagram of the experimental setup is shown in Figure 3.10. A scaled-down prototype of the SC bank is developed in the laboratory using the Wurth Elektronik make SCs. The total of seven SCs are considered for the experiments, three of them are connected in series combination to form the main bank (16.67 F, 8.1 V), the other four are arranged in the auxiliary bank (50 F, 2.7 V) with a series-parallel switching circuitry holding the total energy of 722 J (0.21 Wh). The switching circuit is developed using 6 active MOSFETs (IPW65R070C6) with the isolated gate driver modules (Si8284) to facilitate both the charge and discharge operations. A three-stage switching controller is developed using analog circuits (Op-amps) to drive the gate driver modules.

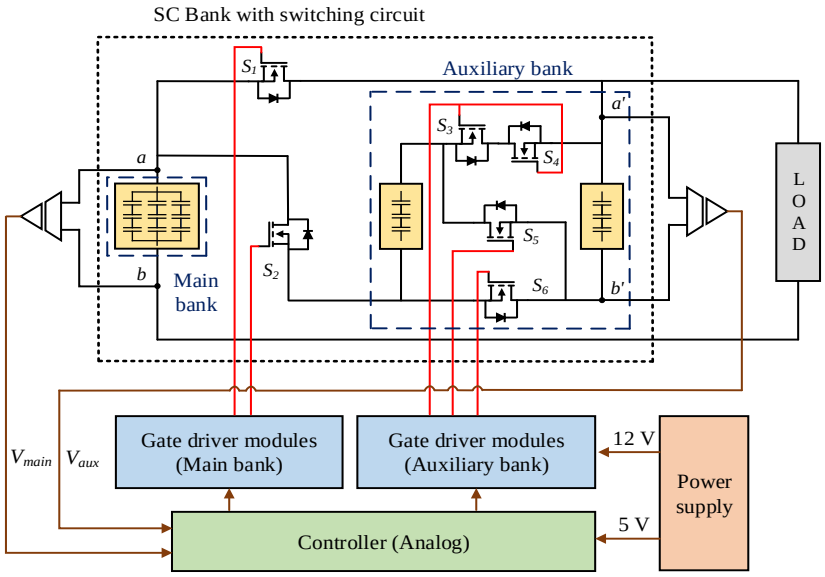

Figure 3.10. Block diagram of the experimental setup.

3.4.1. Charge Characteristics

The initial minimum voltage of the proposed SC bank setup is set to 2.5 V. As the maximum rated voltage of the developed SC bank is 8.1 V, the power supply with a constant voltage of 8.5 V is considered for the charging. A protective resistor of 0.5 Ω is connected in series with the supply to limit the input charge currents. The experimental results of the proposed SC bank during the charge operation is shown in Figure 3. 11.

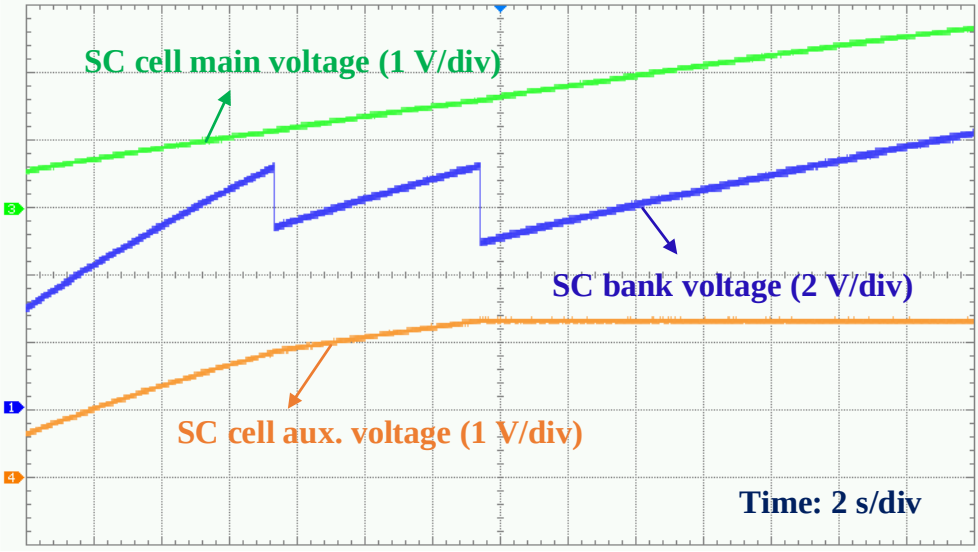

Figure 3.11. Experimental results of the proposed SC bank during charge.

The test results show that the bank voltage is raised from 2.5 V to its maximum rated voltage of 8.1 V and takes 28 s to fully charge the SCs in a bank. Moreover, the auxiliary bank is charged in 13 s and is disconnected from the main bank. As the auxiliary bank is in parallel form, the ESR of the SC bank is reduced (0.12 mΩ). Therefore, the auxiliary bank voltage is maintained at the maximum voltage even after disconnected from the main bank. On the other hand, the SC cell in the main bank is charged from 0.6 V to 2.7 V. Overall, the experimental results show that the time taken for the proposed circuit during charging is similar to the non-switched SC bank.

3.4.2. Discharge Characteristics

To coincide with the simulation results, the considered maximum and minimum voltages of the proposed SC bank for the discharge experiments are 7.6 V and 4 V respectively. A constant resistive load of 1 Ω is used to discharge the bank to its minimum voltage. The experimental results of the proposed SC bank switching circuit during discharge are shown in Figure. 3.12. The test results are compared with the discharge characteristics of the non-switched SC bank prototype comprising 722 J (approx.) of energy as discussed in Chapter 2 (Figure 2.13).

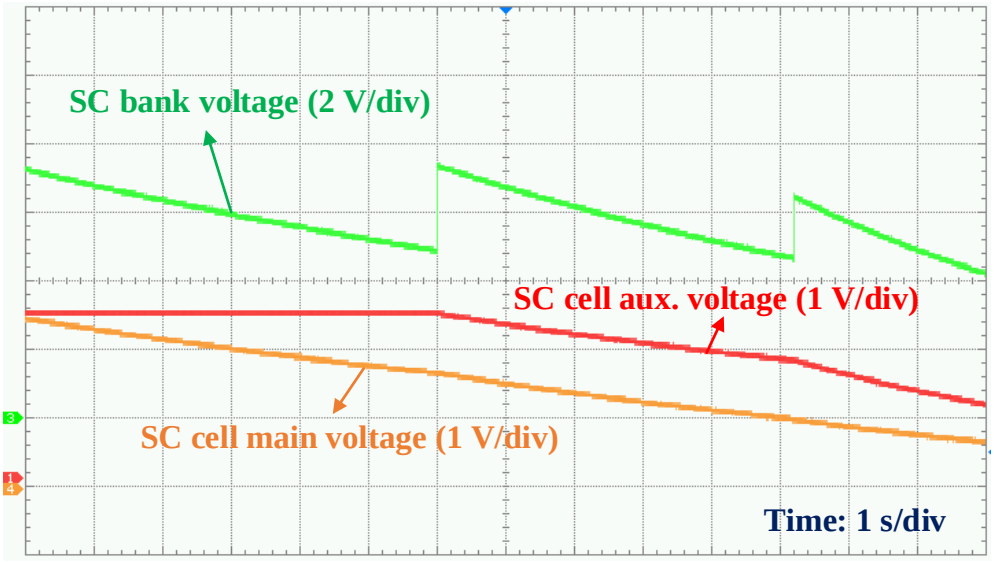

Figure 3.12. Experimental results of the proposed SC bank during discharge.

The results show that the voltage of the SC stack without any switching circuit drops to the 4 V in 12.5 s. Whereas, the SC bank with the proposed switching configuration takes 14 s.

Hence, it is evident that a higher power delivery duration of the bank is achieved with the proposed bank switching circuit. Furthermore, the cell voltage of the SC bank without any switching is discharged to 1.4 V whereas the SC cell voltages of main and auxiliary banks in the proposed bank switching approach are discharged to 0.65 V and 1.1 V, respectively. Hence, the implementation of the proposed switching circuit in the SC bank extracts the left-over energy by deep discharging all SCs of main bank to 0.65 V offering 94.2% of energy utilization efficiency. A comparative analysis of the proposed SC bank with the regular SC bank (no switching) and the conventional SC bank switching method for simulations are summarized in Table 3.3.

Table 3.3. Comparative study on bank switching techniques during discharge

SC bank switching method	**Power delivery time (s)**	**SC cell energy utilization (%)**
Without switching	125.7	72
Conventional [33]	142 (**12% ↑**)	92 (**20% ↑**)
Proposed	148 (**15% ↑**)	95 (**23% ↑**)

3.5. Cost Analysis

Typically, the SC bank with an extra switching circuitry results in increasing the overall system costs. Addressing this issue, a detailed cost analysis of the proposed architecture is performed and compared with the conventional and non-switched SC banks. Assuming the SC banks in all the conventional methods have the same initial energy i.e. 11.2 kJ. In order to implement the SC banks with different switching circuits for a specific application, a detailed cost report is developed as shown in Table 3.4.

The data indicates that the non-switched SC bank with 72% bank efficiency costs $438.04. Whereas the SC bank with a switching circuitry offers high system efficiency (>90%) which costs $738.94. Furthermore, the part count and cost of the proposed architecture are 25% less than the conventional switching approach i.e. $556.64. Therefore, the proposed architecture enhances the power delivery duration and total power density of the SC bank with an additional cost of $118.6 compared to the non-switched SC bank.

Table 3.4. Cost analysis of bank switching techniques

S.no.	Hardware	Part	Unit Price (CAD)	Non-switched SC bank		Conventional SC Bank Switching [33]		Proposed SC Bank Switching	
				Part Quantity	Price (CAD)	Part Quantity	Price (CAD)	Part Quantity	Price (CAD)
1	SCs	300 F, 2.5 V	$36.42	12	$437.04	12	$437.04	9	$327.78
		450 F, 2.5 V	$38.44	0	$0.00	0	$0.00	2	$76.88
2	Switching circuit	MOSFETs	$11.78	0	$0.00	12	$141.36	6	$70.68
3		Diodes	$0.04	0	$0.00	3	$0.12	0	$0.00
4	Gate Driver Circuit	Opto Couplers	$1.77	0	$0.00	12	$21.24	6	$10.62
5		Isolated Power supply	$9.45	0	$0.00	12	$113.40	6	$56.70
6		Diodes (IN4007, IN4148)	$0.04	0	$0.00	12	$0.48	6	$0.24
7			$0.16	0	$0.00	12	$1.92	6	$0.96
8		Capacitors	$0.08	0	$0.00	12	$0.96	6	$0.48
9		Resistors (330, 1K, 10K)	$0.02	0	$0.00	12	$0.24	6	$0.12
10			$0.02	0	$0.00	12	$0.24	6	$0.12
11			$0.01	0	$0.00	12	$0.12	6	$0.06
12		Buffers	$1.38	0	$0.00	12	$16.56	6	$8.28
13	Voltage Sensor	Op-Amp	$0.92	1	$0.92	1	$0.92	1	$0.92
14		Resistors (10K, 5K, 1K)	$0.01	2	$0.02	2	$0.02	4	$0.04
15			$0.02	2	$0.04	2	$0.04	4	$0.08
16			$0.01	2	$0.02	2	$0.02	4	$0.04
17	Controller	Op-Amp	$0.92	0	$0.00	1	$0.92	1	$0.92
18		Not-Gate	$1.41	0	$0.00	1	$1.41	1	$1.41
19		Resistors (18.9K, 1.2K, 7.2K, 12.7K)	$0.26	0	$0.00	1	$0.26	1	$0.26
20			$0.01	0	$0.00	1	$0.01	1	$0.01
21			$0.02	0	$0.00	1	$0.02	1	$0.02
22			$0.02	0	$0.00	1	$0.02	1	$0.02
23		OR-Gate	$1.03	0	$0.00	1	$1.03	0	$0.00
24		XOR-Gate	$0.59	0	$0.00	1	$0.59	0	$0.00
Total					**$438.04**		**$738.94**		**$556.64**

3.6. Summary

The chapter briefs about a new low-cost bank switching architecture for SCs with enhanced energy delivery. A comparative analysis is performed with conventional and non-switched SC banks in terms of power delivery duration, SC energy utilization, and system efficiency. The results show that the proposed SC bank offers a 23% increase in the SC energy utilization efficiency and a 15% rise in power delivery duration compared to the non-

switched SC bank during discharge. Whereas the conventional bank switching approach offers only a 12% increase in power delivery time. On the other hand, a detailed loss and cost analysis is performed. It is noticed that the average power loss of the proposed technique due to switching is 51% lesser than the conventional approach. Furthermore, the overall cost of the proposed system is reduced by 25% compared to the conventional SC bank system.

The terminal voltage of the SC bank is widely varied during charge and discharge operations. Thus, a power converter is associated with a bank that accepts the wide voltage variations at the input and provides a stable voltage at the output. However, the switched SC bank results in high voltage fluctuations. Hence, it is essential to analyze the impact of SC bank switching on the power converter interface. Furthermore, the advantages and drawbacks of using the proposed SC bank with a dc-dc power converter are discussed in the next chapter.

Chapter 4

Bank Switched Supercapacitors with Power Converter

An SC bank in the HESS application always coupled with a bidirectional dc-dc electronic interface to facilitate seamless charging and discharging operation. To verify the appropriateness of the proposed SC bank in HESS, a detailed analysis of bank switched SCs with a constant power load is conducted in this chapter. A bidirectional dc-dc power converter is considered for the load. A brief discussion on modeling and working behavior of a bidirectional dc-dc converter is presented. Furthermore, the impact of a switched SC bank on active and passive devices of the power converter is studied in detail.

4.1. Necessity of a Power Converter

Typically, the energy stored in SCs has a direct relation with its internal voltage. As discussed in the previous chapter, the commercially available SCs are rated from 1.5 V to 3 V and are stacked up in series to meet the load voltage requirements. Thus, the terminal voltage of SCs varies widely from maximum to minimum rated voltage and vice versa in shorter periods during charge and discharge operations. However, this behavior of SC bank deficits in providing a constant dc-link voltage at the output which is essential in hybrid energy storage applications. On the other hand, the SC bank in HESS will charge from dc bus voltage without any control over the charge currents and results in overcharging of SCs. Therefore, a power electronic converter is connected to the SC bank in HESS applications that accepts wide terminal voltage variations at the input and shapes the voltage as a constant at the output.

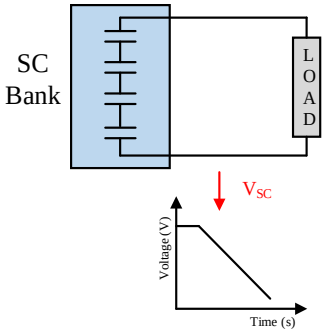

(a)

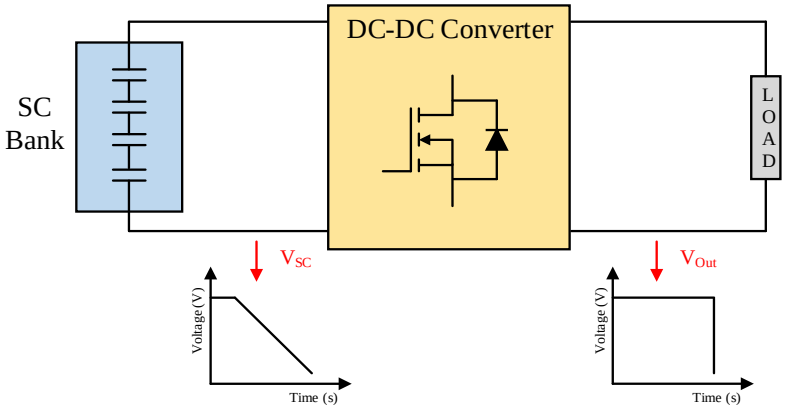

(b)

Figure 4.1. SC bank (a) without power converter and (b) with a power converter.

As a result, the SC bank in HESS is charged or discharged by controlling the charge and discharge currents. The block diagram of SC bank with and without converter is shown in Figure 4.1.

4.2. Bidirectional DC-DC Converter

The Bi-directional dc-dc converters are the most widely used power converters that enable the power flow in both the directions i.e. by operating as a boost converter in one way and buck mode on the other. These are highly used in renewable energy storage [46], FC systems [47], and other hybrid energy storage applications [48]. Moreover, these converters have gained a greater interest in electric vehicular applications by associating with SC banks which facilitates the simultaneous charge and discharge operations with respect to the transient load power demands. Several converters enable the bidirectional power flow that includes Cuk converter, buck-boost converters, half-bridge, and full-bridge converters. These are employed in different applications with different requirements. Among them, the half-bridge bi-directional dc-dc converter is the most widely used power interface in HESS applications due to its low cost and less complex control compared to the other converters [49]. The circuit diagram of the half-bridge dc-dc converter is shown in Figure 4.2.

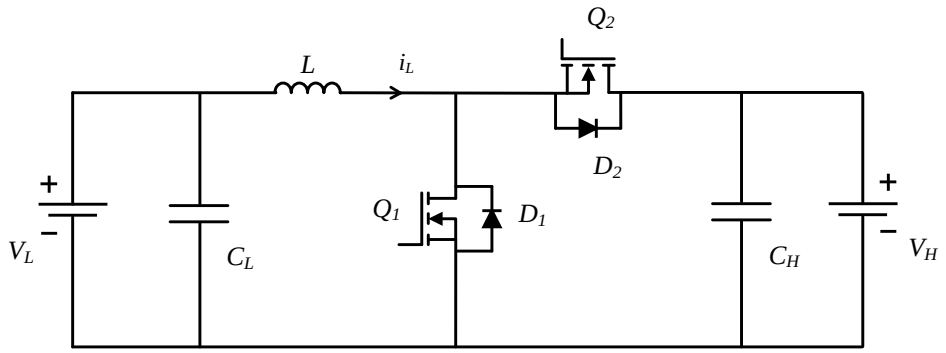

Figure 4.2. Half-bridge bidirectional dc-dc converter.

Typically, a conventional buck and boost converters comprise a diode that enables a unidirectional power flow. The diodes are now replaced by the MOSFETs to form a bidirectional switch and allow the current conduction in both the ways. Therefore, the half-bridge dc-dc converter replicates the anti-parallel combination boost and buck converter

with an additional bidirectional power flow feature [50]. The circuit consists of two active switches Q_1 and Q_2 associated with an individual free-wheeling diodes D_1 and D_2, respectively. The switches are operated to perform the step-up or step-down operation of the applied voltages as per the load demands. The modes of operation of the bi-directional dc-dc converter are shown in Figure 4.3(a), (b), (c), and (d) respectively.

In boost mode of operation, the switch Q_1 and diode D_2 are conducted. Whereas the other devices Q_2 and D_1 are in OFF state. At this stage, the switch Q_1 is turned ON and the current through the inductor increased until the gate pulse is zero. The current flow in the converter is shown in Figure 4.3(a). When the switch Q_2 is turned OFF, the diode D_2 is forward biased and the inductor current charges the high-side capacitor C_H as shown in Figure 4.3(b). In buck mode of operation, the switch Q2 and diode D1 are in conduction whereas the switch Q1 and diode D2 are inoperative.

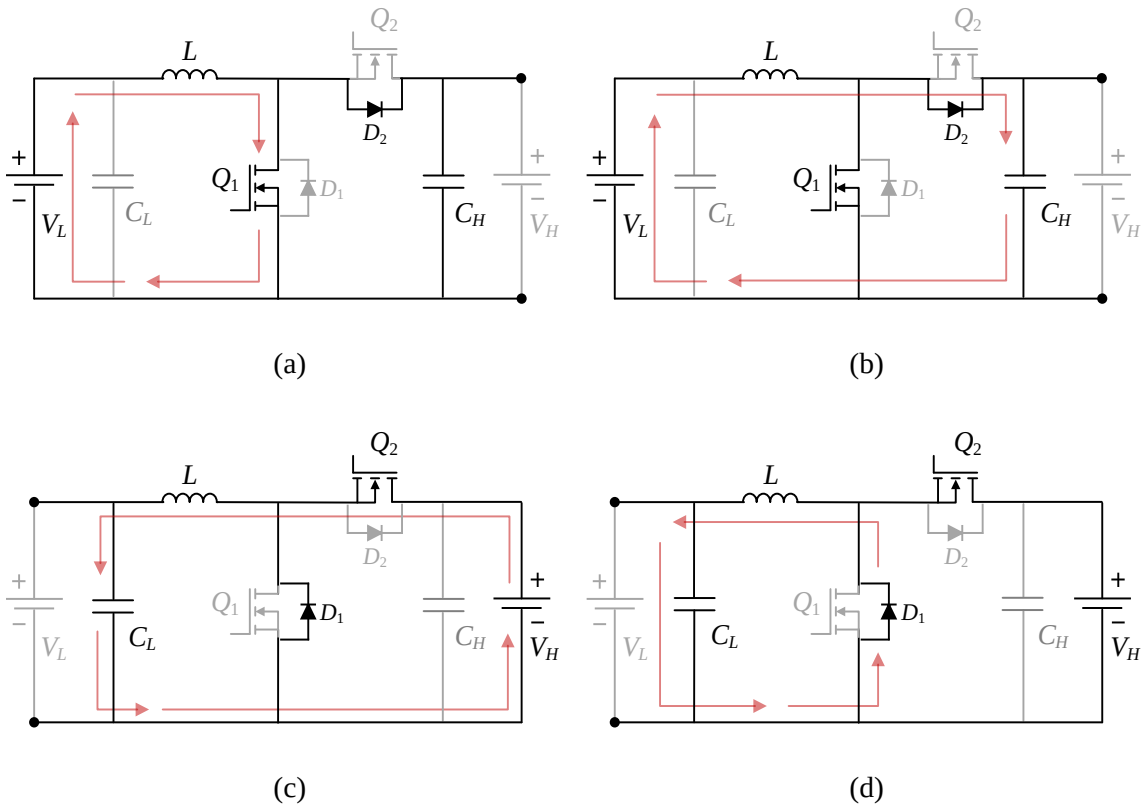

Figure 4.3. Bi-directional dc-dc converter operation during (a), (b) Boost mode, and (c), (d) Buck mode.

At this stage, the switch Q_2 is turned ON and the higher side voltage (V_H) will charge the inductor as shown in Figure 4.3(c). The switch Q_2 is turned OFF as per the duty ratio and the inductor current is discharged onto the battery. The free-wheeling diode D_2 is conducted and creates the path for the current flow as shown in Figure 4.3(d).

4.2.1. Modeling of Bidirectional DC-DC Converter

Typically, the SC bank is connected to the lower side of the aforementioned half-bridge power converter i.e. $V_{SC} = V_L$, where it steps up the voltage (V_L) during discharge and steps down the higher side voltage (V_H) during the charging operation. The converter is modeled in accordance with the application and assuming that it is operated in CCM during discharge i.e. the inductor current is always greater than zero ($I_L > 0$). For instance, the inductor current (I_L) of the power converter in boost mode operating in CCM is shown in Figure 4.4.

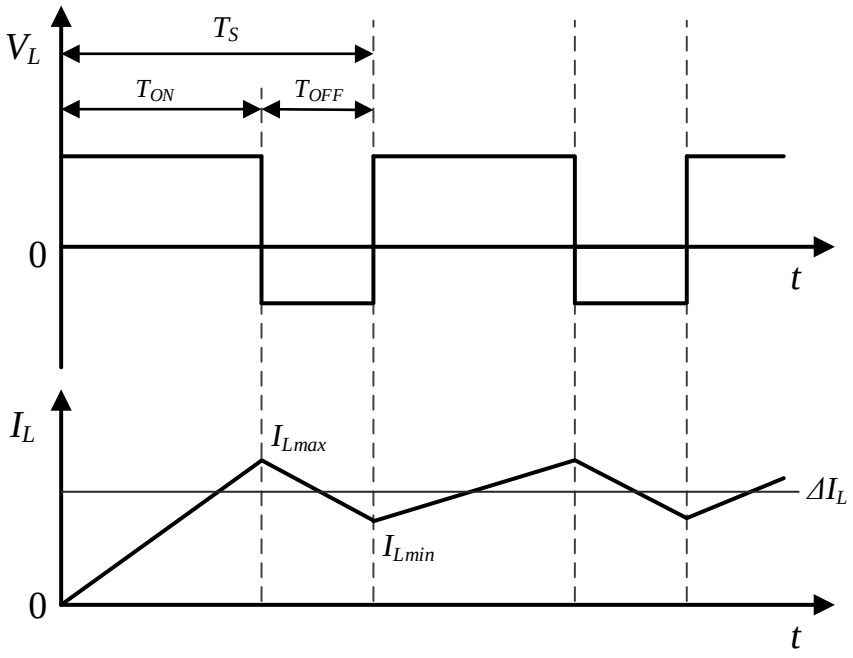

Figure 4.4. Inductor current of the bidirectional dc-dc converter in CCM.

Where D is the duty ratio of the power converter, T_s is the total switching period, and ΔI_L is the current ripple. The gate pulse voltage V_g is constant during ON and OFF periods. Thus, the inductor current is a linear ramp signal as shown in Figure 4.4.

The respected equations of duty cycle during OFF (4.1) and ON (4.2) are given as,

$$1 - D = \frac{T_{OFF}}{T_S} \tag{4.1}$$

$$D = \frac{T_{ON}}{T_S} \tag{4.2}$$

Considering the power converter with zero losses, the voltage drops across the MOSFETs and diodes are neglected for the analysis.

1. *Boost Mode (Discharge):*

   From the aforementioned modes of operation, the switch Q_1 and diode D_2 are in conduction mode. The current ripple of the inductor when Q_1 is turned ON i.e.,

$$\Delta I_{L1a} = \frac{(V_L)T_{ON}}{L} \tag{4.3}$$

   When the switch Q1 is turned OFF, the ripple is given by,

$$\Delta I_{L2a} = \frac{(V_H - V_L)T_{OFF}}{L} \tag{4.4}$$

   Equating (4.3) and (4.4),

$$(V_L)T_{ON} = (V_H - V_L)T_{OFF} \tag{4.5}$$

   Dividing both sides by the total switching period (T_S) and substituting the equations (4.1) and (4.2) we get,

$$V_H = \frac{V_L}{1 - D} \tag{4.6}$$

2. *Buck Mode (Charge):*

   In similar to the boost operation, the switches Q_2 and diode D_2 are in conduction. The current ripple when the switch Q_2 is turned ON is given by,

$$\Delta I_{L1b} = \frac{(V_L - V_H)T_{ON}}{L} \tag{4.7}$$

   When the switch Q_1 is turned OFF, the current ripple is given by,

$$\Delta I_{L2b} = \frac{(V_H)T_{OFF}}{L} \tag{4.8}$$

   To derive V_H, the equations (4.3) and (4.4) are equated as,

$$(V_L - V_H)T_{ON} = (V_H)T_{OFF} \tag{4.9}$$

Dividing both the sides by T_S and substituting (4.1) and (4.2) we get,

$$V_H = (D)V_L \tag{4.10}$$

Hence the output voltage (V_H) is directly related to the duty cycle of the gate pulses in CCM mode of operation.

4.2.2. Inductor and Capacitor Design

The inductor for the bidirectional dc-dc converter is selected with respect to the current ripple. Usually, the converter operating in CCM mode acquires less current ripple. Thus, resulting in larger size inductors. The critical inductance of the buck and boost converter depends on the steady-state duty cycle, switching period and the load resistance values are given by,

$$L_{Boost} = \frac{(1-D)^2 D * T_S * R_{Load}}{2} \tag{4.11}$$

$$L_{Buck} = \frac{(1-D) * T_S * R_{Load}}{2} \tag{4.12}$$

Therefore, the minimum inductance of the power converter is,

$$L = min[L_{Boost}, L_{Buck}\,] \tag{4.13}$$

The ripple current of the is given by,

$$\Delta I = \frac{1}{2} * \frac{(V_H - V_L)}{L} * \frac{V_L}{V_H} * T_S \tag{4.14}$$

The mean value of the inductor current of the is given by,

$$I_{RMS} = \sqrt{I_{Load}^2 + \frac{\Delta I^2}{3}} \tag{4.15}$$

Moreover, the input and output capacitor values from the lower side and higher side voltage ripple (ΔV_L and ΔV_H) is given as,

$$C_L = \frac{\Delta I * T_S}{8 * \Delta V_L} \tag{4.16}$$

$$C_H = \frac{V_L * D * T_S}{R_L * \Delta V_H} \tag{4.17}$$

4.3. State-space Averaged Model

In order to perform the state-space averaging model, A complimentary gating signal for the considered single-phase converter is applied as shown in Figure 4.5. As discussed, two voltage sources i.e. on the higher side (dc-link voltage) and lower side (SC bank voltage) are included in the model. The switches Q_1 and Q_2 are used to control the converter in compliance with boost (discharge) and buck mode (charge) of operation. In buck mode, the negative current created by the switch Q_1 helps charge the input capacitor C_L. If the capacitor is fully charged, the body diode D_2 carries the negative inductor current. Once the MOSFET Q_2 is turned ON, the current flow is reversed. The dead time in the gating signal is represented as t_d.

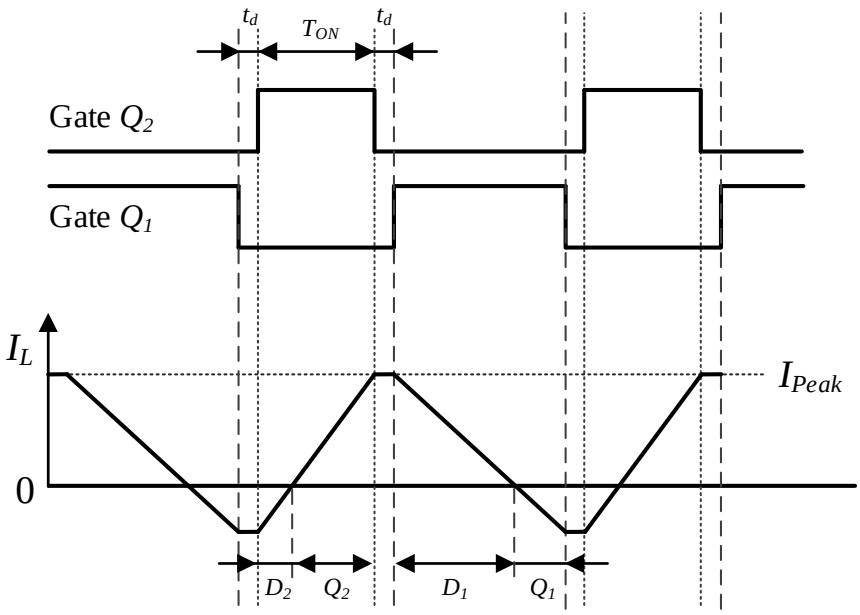

Figure 4.5. Complimentary gating signal control.

The state-space averaged model of the bidirectional dc-dc converter is implemented with the following assumptions.

1. The switching frequency of the converter is 10 kHz i.e. the switching period is 100 ms. The dead time considered as 1 ms. Therefore, the deadtime period is neglected.
2. The soft switching period in the gating signal is very low. Thus, it is neglected for the analysis.

3. The turn ON resistance of the MOSFET is assumed to be the same during both the charge and discharge operations.

The ESR of the SC bank at the lower side and the internal resistance of the dc-link voltage at the higher side are considered as R_1 and R_2 respectively. Moreover, the turn on-resistance of the MOSFET is R_{SON}. The parasitic resistance of the inductor is R_{PL} is included in the model. To enable the power flow in both the directions, the averaged inductor current (I_L) or the averaged load current (I_{Load}) is considered for discharge or charge operation. Irrespective of the operating modes, the converter has two subintervals. The first subinterval operates when Q_1 is ON and Q_2 is OFF as shown in Figure 4.6(a). On the other hand, the second subinterval is operated when the switches Q_1 is OFF and Q_2 is on as shown in Figure 4.6(b).

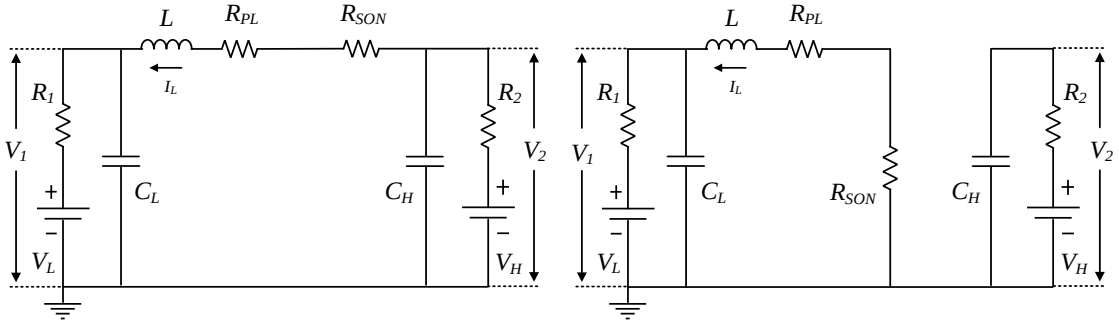

Figure 4.6. Bidirectional dc-dc converter with (a) first and (b) second subintervals.

The state-space model of the bidirectional dc-dc converter is given as (4.18),

$$0 = A.\begin{bmatrix} I_L \\ V_2 \\ V_1 \end{bmatrix} + B.\begin{bmatrix} V_L \\ V_H \end{bmatrix} \tag{4.18}$$

Where,

$$A = \begin{bmatrix} -\frac{R_P}{L} & \frac{D}{L} & -\frac{1}{L} \\ -\frac{D}{C_H} & -\frac{1}{R_2.C_H} & 0 \\ \frac{1}{C_L} & 0 & -\frac{1}{R_1.C_L} \end{bmatrix}, \text{B}= \begin{bmatrix} 0 & 0 \\ 0 & \frac{1}{R_2.C_H} \\ \frac{1}{R_1.C_L} & 0 \end{bmatrix}, \text{ and}$$

$$R_P = R_{PL} + R_{SON}$$

By solving (4.18) we get,

$$I_L = \frac{D.V_H - V_L}{L} \tag{4.19}$$

$$V_1 = \frac{D.(V_H.R_1 + D.R_2.V_L) + R_P.V_L}{R_2.D^2 + R_1 + R_P} \tag{4.20}$$

$$V_2 = \frac{V_H.(R_1 + R_P) + D.R_2.V_L}{R_2.D^2 + R_1 + R_P} \tag{4.21}$$

Since all the parameters are considered as constant, each subinterval of the converter acts like the time-invariant system. However, the converter behaves as the time-varying system during the transition between two modes. Thus, the state space averaging used to approximate the converter to obtain the continuous linear time-invariant system. The state-space averaged model of the bidirectional converter is given by,

$$\frac{d}{dt}\begin{bmatrix}\hat{\imath}_L \\ \hat{v}_2 \\ \hat{v}_1\end{bmatrix} = A.\begin{bmatrix}\hat{\imath}_L \\ \hat{v}_2 \\ \hat{v}_1\end{bmatrix} + C.\begin{bmatrix}I_L \\ V_2 \\ V_1\end{bmatrix}.\hat{d} \tag{4.22}$$

Where,

$$C = \begin{bmatrix} 0 & \frac{1}{L} & 0 \\ -\frac{1}{C_H} & 0 & 0 \\ 0 & 0 & 0 \end{bmatrix}$$

Thus, the transfer function to obtain the relationship between high side dc bus, low side SC bank voltage, inductor current, and duty ration is given by,

$$\frac{\hat{v}_1}{\hat{d}} = \frac{\frac{1}{C_L}}{s + \frac{1}{C_L.R_1}} . \frac{\hat{\imath}_L}{\hat{d}} \tag{4.23}$$

$$\frac{\hat{v}_2}{\hat{d}} = \frac{-\frac{D}{C_H}.\frac{\hat{\imath}_L}{\hat{d}} - \frac{1}{C_H}.I_L}{s + \frac{1}{C_H.R_2}} \tag{4.24}$$

$$\frac{\hat{\imath}_L}{\hat{d}} = \frac{(a_0 s + 1)[(a_1 s + 1).V_2 - a_2]}{(L.s + R_P)(a_0 s + 1)(a_1 s + 1) + D^2 R_2(a_0 + 1) + R_1(a_1 s + 1)} \tag{4.25}$$

Where,

$$a_0 = C_L.R_1,\ a_1 = C_H.R_2,\ a_2 = D.I_L.R_2$$

Therefore, the parameters of the bidirectional converter and the steady-state value of *V* and *I* are substituted in the equation (4.25) to acquire the gains of the PI controller.

4.4. Impact of Bank Switching on a Power Converter

Typically, a non-switched SC bank is allowed to discharge from its maximum to minimum rated voltage using a constant resistive load result in high voltage variations at the terminals. As a concern, a power converter is designed and connected to the SC bank that accepts such voltage variations and delivers a constant voltage at the output. However, the current stress on active and passive devices of a power converter rises with the reduction of SC bank voltage during discharge. The higher the terminal voltage variation, the maximum ratings of active and passive devices are used to design a power converter. Moreover, the switching and conduction losses across the switches are increased which affects the overall system efficiency of the power converter.

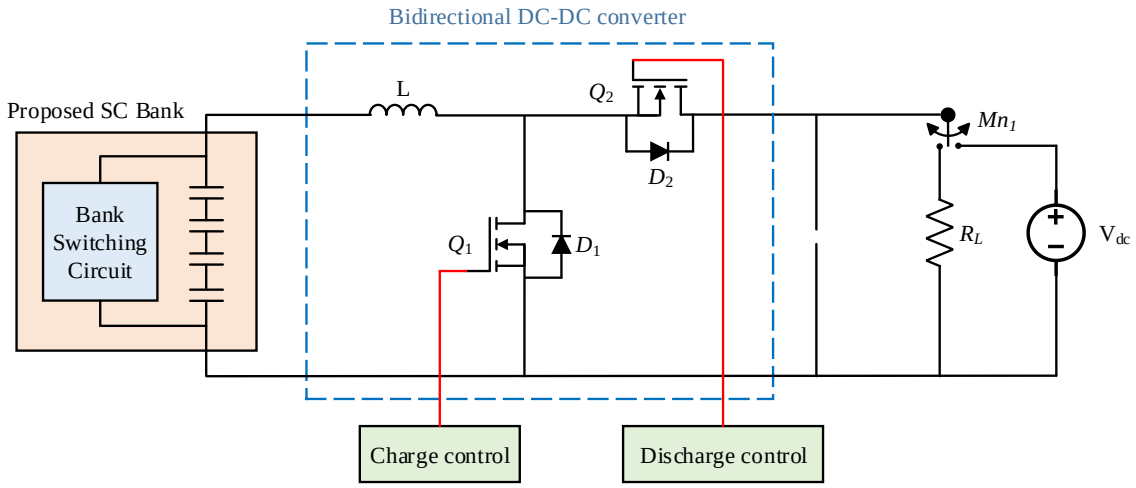

Figure 4.7. Proposed SC bank with a bidirectional dc-dc power converter.

Addressing this issue, the proposed SC bank circuit is connected to a bidirectional power electronic converter for the analysis. As discussed in the previous chapter, the SC bank with a switching circuit results in lower voltage fluctuations (ΔV) i.e. limited to 36%

compared to the SC bank without any switching and delivers the maximum power delivery duration during discharge. On the other hand, the charge characteristics of the proposed SC bank offers the same ΔV and is maintained within the threshold limits. The block diagram of the proposed SC bank switching circuit with a bidirectional dc-dc converter is shown in Figure. 4.7. The main switch (Mn_1) is used to discharge and recharge the SC bank using the bidirectional dc-dc power converter.

4.5. Simulations and Analysis

The impact of bank switching on a power electronic interface is verified by conducting the simulation studies on the PLECS software platform. At first, the proposed SC main (7.5 V, 300 F) and auxiliary (2.5 V, 900 F) banks are connected to a synchronous bidirectional dc-dc converter. Besides, a non-switched SC bank (7.5 V, 400 F) with the same energy is considered for the simulation studies.

4.5.1. Inductor Current Variation

The inductor current of the power converter is considered for the analysis to verify the impact of SC bank terminal voltage variations. The non-switched SC bank and the proposed SC banks are connected to the bidirectional dc-dc power converter and allowed to discharge using a constant resistive load of 1 Ω. To regulate a constant 10 V at the output, the closed-loop control is implemented using the PI controller. Since the studies are conducted only for the discharge operation, the switch Q_2 is always in OFF condition. The system parameters of the bi-directional dc-dc converter and the controller gains are shown in Table 4.1.

Table 4.1. System parameters of bidirectional dc-dc converter

DC-DC converter and PI control parameters	
Filter Inductor (L)	800 μH
Filter Capacitor (C_f)	470 μF
Switching Frequency (f_{sw})	10 kHz

The results of the inductor current variation with regard to the SC bank voltage (with and without switching) during the discharge mode of operation is shown in Figure 4.8.

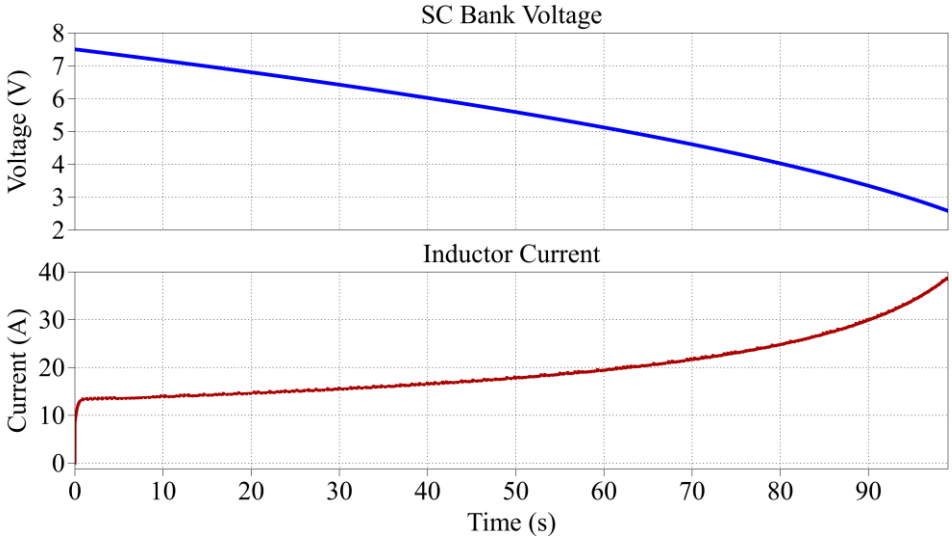

(a)

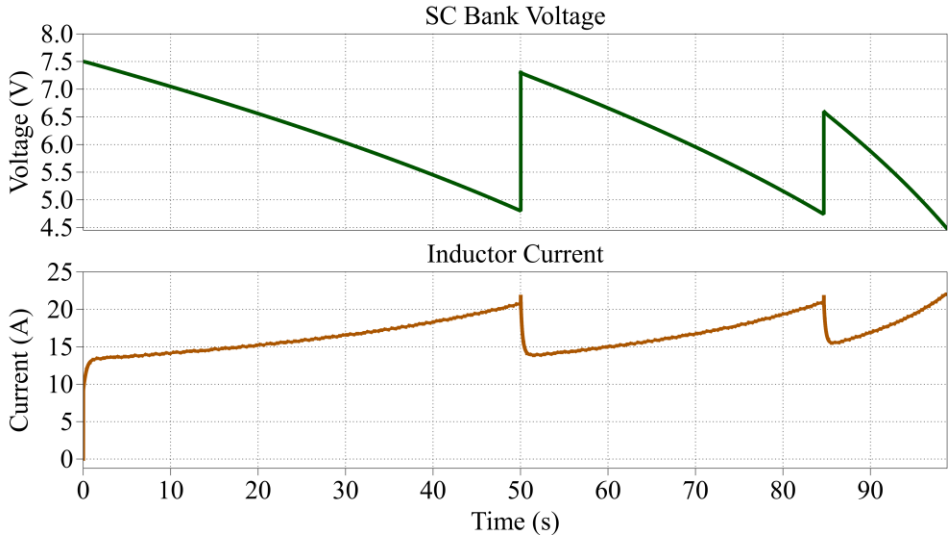

(b)

Figure 4.8. Inductor current variation of (a) Non-switched SC bank and (b) Proposed SC bank switching method.

To regulate a constant voltage of 10 V for 100 s, the inductor current in the dc-dc converter connected to the SC bank without any switching is reaches to 40 A. On the other hand, the inductor current of the power converter with proposed SC bank switching circuit is limited

to 22 A. As a result, the current stress on the inductor is significantly reduced. Moreover, the power converter associated with the proposed SC bank switching architecture can be designed with the less rated active and passive devices. Thus, reduces the sizing and cost of the power electronic converter.

4.6. Summary

This chapter explains about the necessity of a power converter for an SC bank in HESS applications. The design and modeling of a half-bridge bidirectional dc-dc power converter are discussed in detail. Furthermore, the proposed SC bank is associated with the designed power converter to analyze the impact of switching on the active and passive devices of the converter. Finally, the inductor is considered for the analysis, and the current through the inductor is monitored during the discharge operation. In addition, the comparative analysis in terms of reduced voltage variations is performed by connecting the non-switched SC bank with the same converter. The results show that the ripple currents of the inductor are reduced by 45% compared to the discharge results of the non-switched SC bank. Therefore, the proposed bank-switching reduces the current stress and enhances the conversion efficiency of the bidirectional converter.

As the SC bank with the bidirectional dc-dc converter is highly utilized in HESS applications, the efficacy of the proposed SC bank with a battery driving an electric propulsion system is studied in the next chapter. The advantage of the maximum power delivery duration and reduced voltage variations offered by the proposed SC bank is discussed by conducting a detailed case study of an EV and discharging the switched SC bank under various driving cycles which are examined in the further chapters.

Chapter 5

Hybrid Energy Storage System: EV Case Study

The previous chapter details about the efficiency of the proposed SC bank with a bidirectional dc-dc power converter during discharge. The inductor current analysis justifies that the proposed SC bank can reduce the sizing and cost of the power converter. This chapter verifies the proposed concept in HESS by integrating the battery to drive an electric propulsion system. A detailed case study on a small EV is performed under various standard driving cycles. A comparative study carried out with the non-switched SC bank in HESS. The proposed architecture in terms of SC bank terminal voltage variations, SoC, and DoD is analyzed and discussed in detail.

5.1. Introduction

The widely used EVs, HEVs, and PHEVs comprise of a Li-ion battery as the main energy source to drive its electric propulsion system. However, the battery system alone may not be adequate to fulfill peaky load demands and transient load variations. In such cases, the batteries are forced to operate at high discharge rates in shorter periods. This issue can be addressed by employing an oversized battery pack, thereby increasing the number of the depth of discharge/charge cycles, weight, and the cost of the ESS. Furthermore, their aging is accelerated due to periodic charge and discharge, which hassles its replacement before the expected vehicle maintenance [51].

On the other hand, SCs possess a high specific power density, longer lifecycle, and the ability to operate at extremely low and high temperatures [52]. Due to these salient features, SCs are used in conjunction with the batteries to deal with such pulsating load demands, thus forming a HESS. Moreover, the batteries in HESS are downsized and designed to serve only the smaller transients for a longer duration. As a result, such configuration enhances the driving range of an EV and reduces the power per unit cost. To reduce the energy consumption and to extend the range of an EV, the regenerative braking mode is incorporated in HESS [53]-[55]. The SCs are used to recuperate the energy from regenerative braking and assist the battery in serving high transient power demands [53].

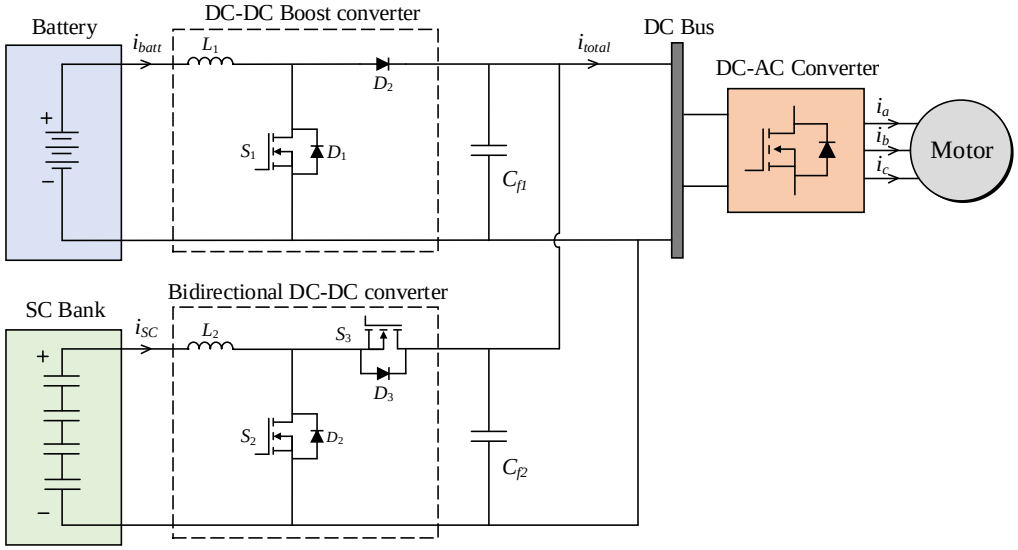

Figure 5.1. Parallel-active battery/SC hybrid energy storage system.

Typically, a power electronic converter is used to combine the batteries and SCs to regulate a constant dc-link voltage that drives an electric powertrain [56]. Several interfacing architectures such as passive-cascaded, parallel-active, and multiple-input systems are used to unite batteries and SCs [57]. Among them, the parallel-active systems are the most popularly used in battery/SC HESS for vehicular applications due to its high voltage gain with a smaller battery pack is shown in Figure 5.1. To verify the charging behavior of the proposed SC bank, a unidirectional boost converter is used at the battery, to step-up the voltages and smoothens its current. On the other hand, SC bank with high cycle life is interfaced with a bidirectional dc-dc converter to facilitate the power flow during charge and discharge. Such configuration allows the battery to supply the mean power and the SC bank to deliver transient power to the load [58].

5.2. Power Management of HESS

The HESS in an EV is operated by employing predefined control schemes for the power electronic converters and the load power allocation. Also, implementing the proposed SC bank architecture in HESS requires an extra switching control with the proper transition by maintaining the SC bank voltage within the threshold limits. The switch control of the power converters is modeled as per the methodology discussed in the previous chapter. However, the load power allocation and band-based switching control are discussed as follows.

5.2.1. Power Allocation Algorithm

In a practical environment, the power demand profile of electric powertrain varies with regard to the driving cycle and other EV parameters such as weight, cross-section, etc. As a result, the load power in HESS is divided and shared between the batteries and SCs to serve the demands. A frequency share-based control algorithm presented in [59] is implemented to allocate the power among battery and SC in accordance to load demand. The total load power is equal to the sum of power allocated to the battery pack and SC bank i.e. given as,

$$P_{Load} = P_{Battery} + P_{SC} \tag{5.1}$$

A second-order Butterworth LPF is used in the control to pass the low-frequency load power components to the battery and the rest of the power to the SCs. The control flow of the frequency share approach is shown in Figure 5.2.

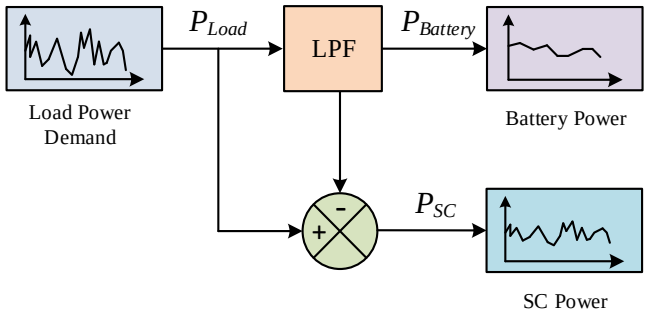

Figure 5.2. Power-sharing control in HESS.

5.2.2. Band-based Bank Switching Control

A three-level band-based control scheme for the proposed switching circuit in HESS is represented in Figure 5.3. Typically, the SC bank voltage is varied from V_{min} to V_{max} and vice versa during the charge and discharge process.

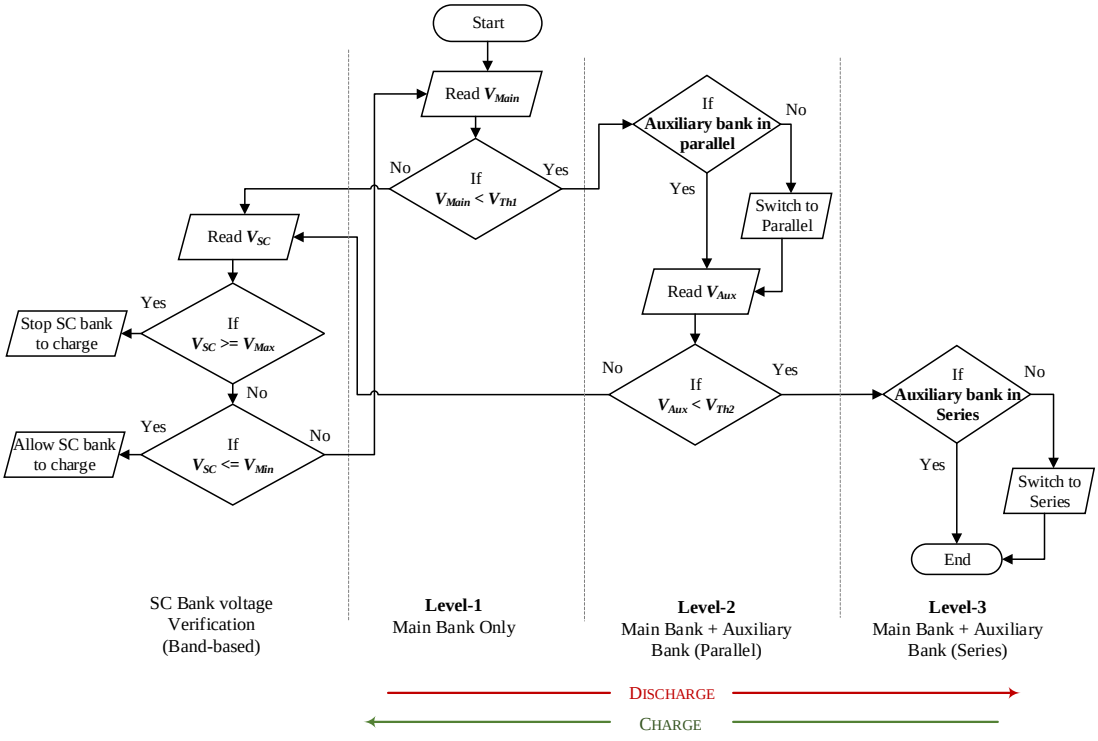

Figure 5.3. Band-based bank switching control in HESS.

To avoid the overcharging of SCs in HESS, the band-based verification check is performed in the control algorithm to maintain the SC bank voltage within the rated thresholds. During the discharge process, only the main bank is allowed to discharge until the first pre-set threshold voltage. The auxiliary bank with a series-parallel changeover circuit is employed to support the main bank while at pulsed load demands. Similarly, during charging, the auxiliary bank in HESS is charged first and then followed by the main bank.

5.3. Battery and Supercapacitors Sizing

The sizing of HESS should offer high specific energy and power densities with the reduced weight of energy storage elements. To accomplish this, the peak power demand of an EV for a specific drive cycle is analyzed. A UDDS drive cycle is considered to size the components in HESS fed EV drive. demand for the selected drive cycle is 22 kW. Assuming only the battery to supply the load demand for a longer time, it is required to provide 14 kWh of energy, and the rest is provided by the SCs. Therefore, the battery is sized at 48 V, 280 Ah and the SC bank is rated 62.5 V, 400 F to maintain a constant 80 V dc-link voltage.

In order to match with the total energy of non-switched SC bank rated 62.5 V, 400 F, the proposed SC bank is sized as per the design equations discussed in Section II. The main bank is rated at 62.5 V, 300 F, and the auxiliary bank is rated at 22.5 V, 900 F considering 36% of voltage variations. The main and auxiliary voltage thresholds for switching are 40 V and 16.65 V, respectively.

5.4. Real-time Simulations: EV Case Study

The real-time implementation of the proposed bank switching technique in a battery-SC HESS for an EV with the selected vehicle parameters (Table 5.1) is carried out. A parallel-active battery-SC power interface (Figure 5.1) is implemented to drive the electric powertrain. The unidirectional boost converter and bidirectional buck-boost converter is modeled and designed based on the ratings of battery and SC banks [60]. The closed-loop control is designed by tuning the PI controller which regulates a constant dc-link voltage at the output. Each converter is employed with an individual PI controller. The overall system parameters considered for HESS are given in Table 5.1.

Table 5.1. HESS System parameters

EV system parameters	
Curb weight (M_K), Passenger weight (M_P)	620 Kg, 120 Kg
Cross-sectional Area (A)	2.6 m^2
The diameter of the wheel (d)	0.62 m
Gear ratio (G)	10.2
Unidirectional & bidirectional dc-dc converter parameters	
Inductor - unidirectional (L_1)	1 mH
Inductor - bidirectional (L_2)	800 µH
DC-link capacitor (C)	470 µF
Switching frequency (f_{sw})	10 kHz
DC-link voltage (V_{DC})	80 V

In HESS, the load power allocation between the battery pack and SC bank is performed using the aforementioned power share algorithm. The cut-off frequency for the LPF is set to 800 mHz. The simulation results of the power allocation for the HWFET drive cycle is shown in Figure 5.4.

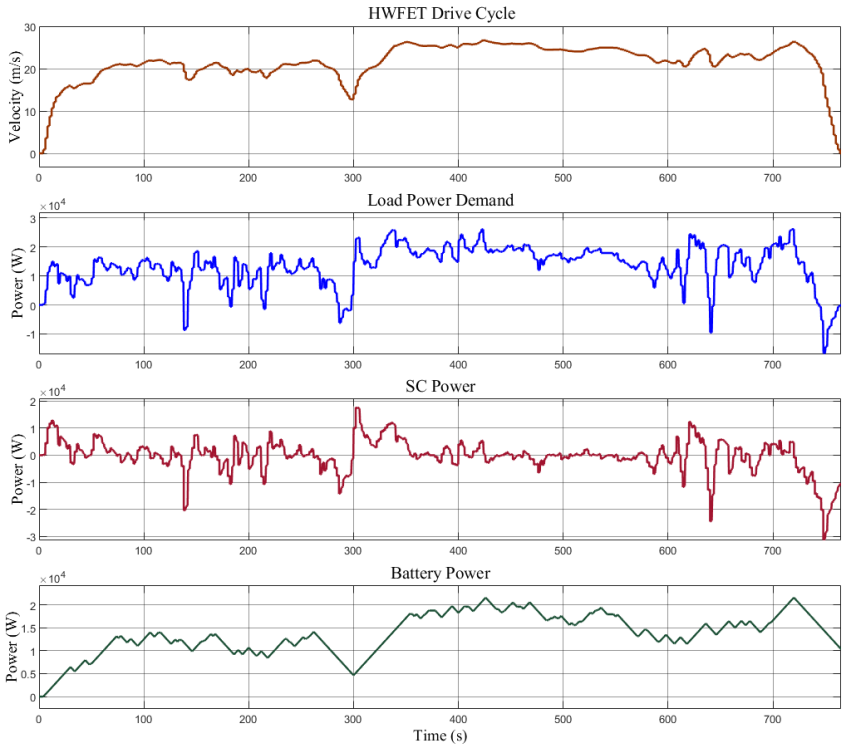

Figure 5.4. Load power allocation results.

5.5. Drive Cycle Analysis and Discussion

The real-time simulations are performed for four different drive cycles such as the UDDS, HWFET, NEDC, and Artemis rural driving cycle.

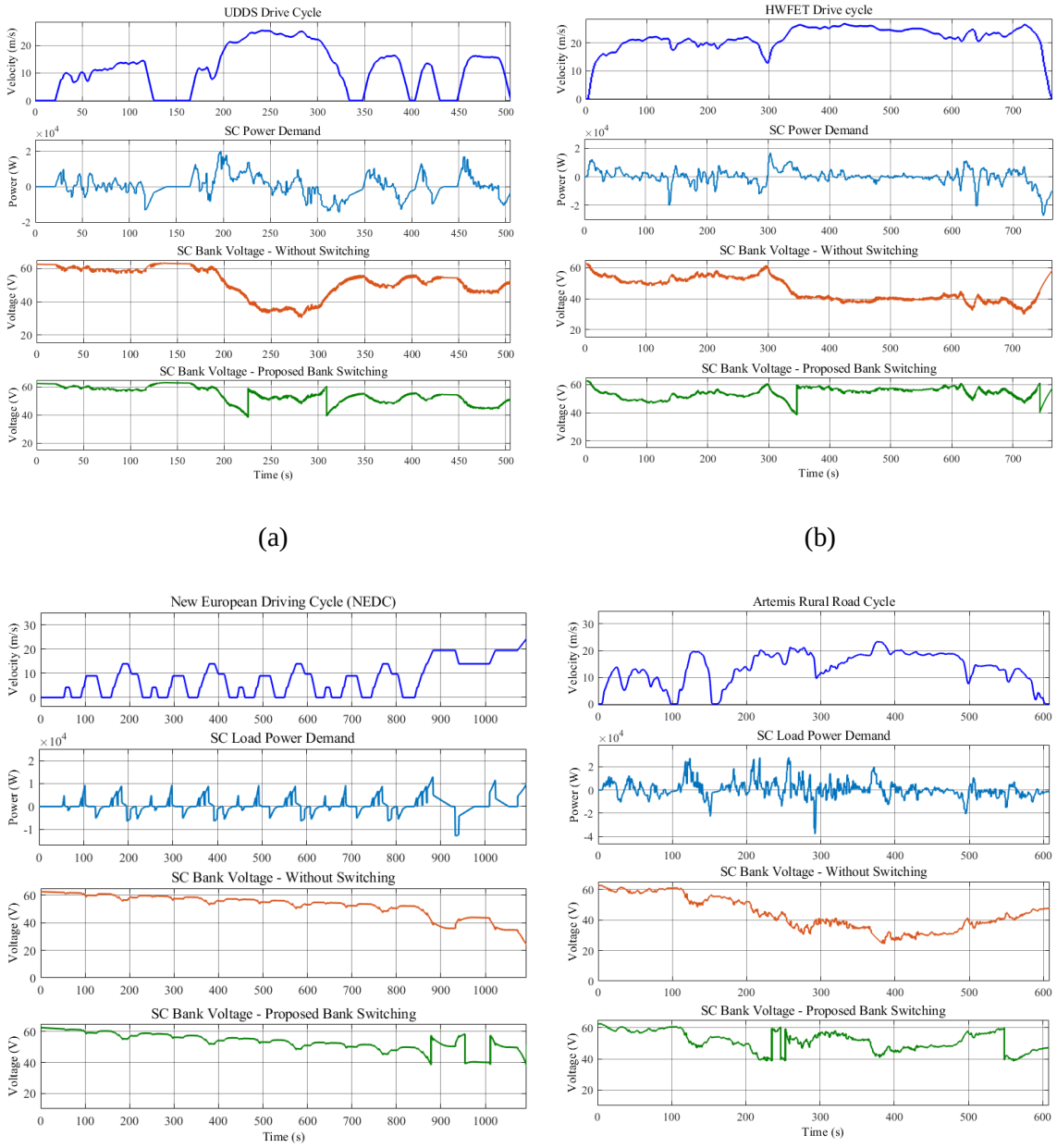

Figure 5.5. SC bank voltage variation with and without proposed bank switching under the (a) UDDS (b) HWFET (c) NEDC and (d) Artemis drive cycle

To verify the effectiveness of the charging process in the proposed SC bank, the charging mode of operation is considered from regenerative braking power.

5.5.1. Terminal Voltage Variations

To verify the terminal voltage variations, a comparative analysis of the proposed SC bank with the non-switched SC bank is performed. The results of the SC bank voltages in HESS under standard UDDS, HWFET, NEDC, and Artemis drive cycles are shown in Figure 5.5 (a), (b), (c), and (d) respectively. The drive cycle results represent that the terminal voltage variations of UDDS pattern for the SC allocated power in the non-switched SC bank is varied from 62.5 V to 31.8 V. On the other hand, the voltage variations of the proposed SC bank switching are maintained within 36% range i.e. from 62.5 V to 40 V. Similarly, it is noticed that the voltage variations for the non-switched SC stack under HWFET drive cycle is varied from 62.5 V to 30 V. However, the SC bank voltage variations in the proposed configuration is maintained within the range of 36% and the same is observed for the NEDC and Artemis rural driving patterns. From the aforementioned test results, the proportion of voltage variations for all the four different drive cycles is compared and summarized with respect to the SC bank with and without bank switching approaches as shown in Figure 5.6.

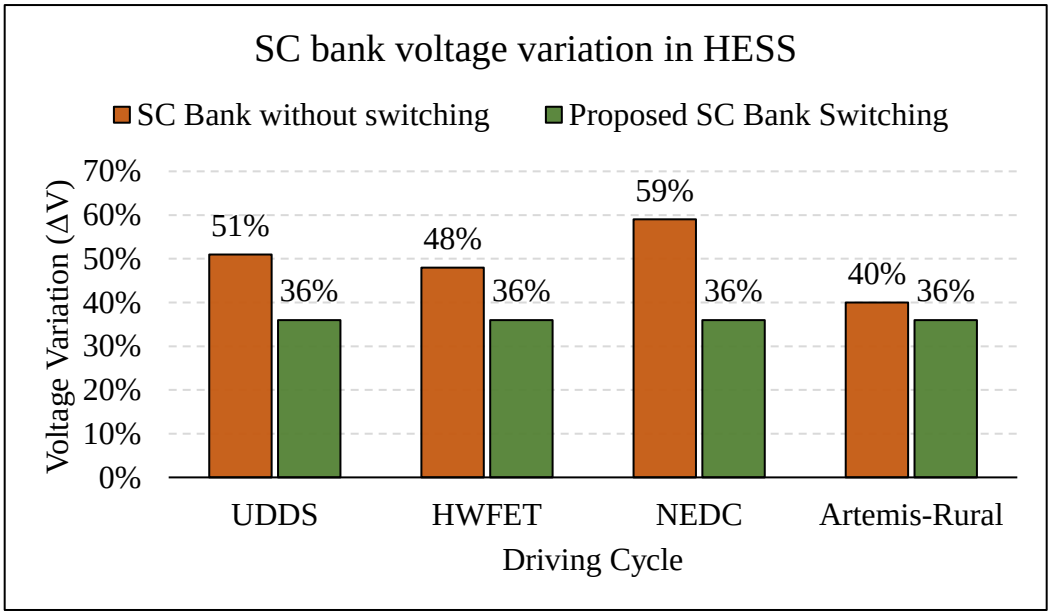

Figure 5.6. SC bank voltage variation analysis in HESS.

The results show that the UDDS driving cycle results in higher SC bank terminal voltage variations. Whereas the Artemis-rural pattern is the lowest compared to the other driving patterns. HESS employing proposed SC bank delivers a constant 36% of voltage fluctuations regardless of the type of driving cycle. Due to the reduction in voltage fluctuations, the conversion efficiency of the bi-directional dc-dc converter is improved.

5.5.2. State of Charge

Typically, an SC bank with high voltage variation discharges quickly and deficits in serving the next series of load transients until it gets charged either from a battery or from the regenerative braking power in HESS.

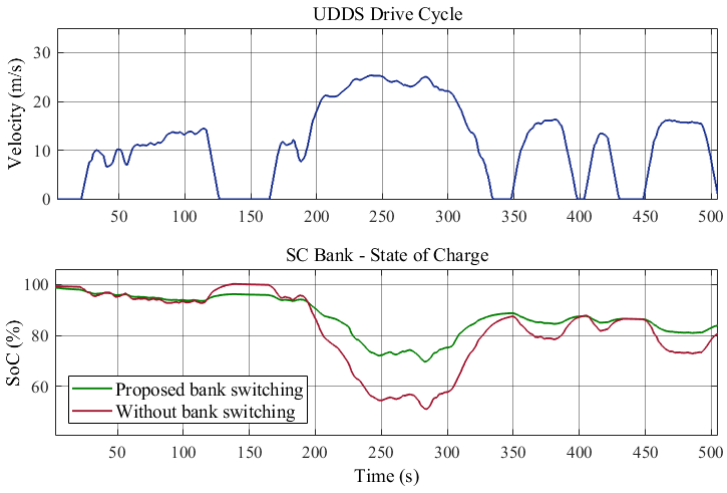

(a)

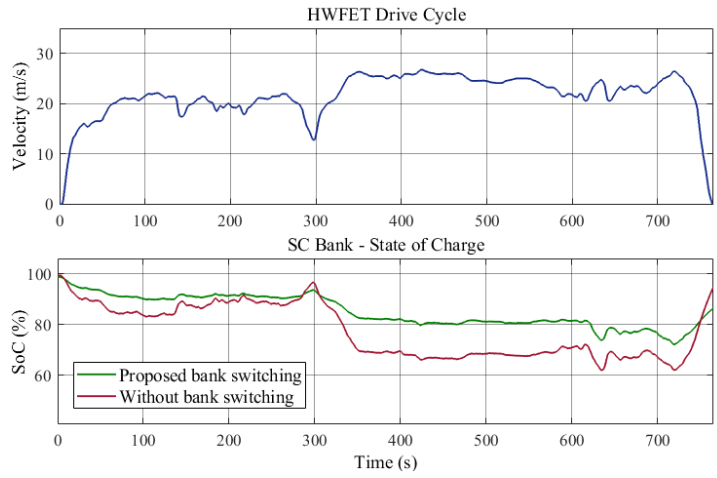

(b)

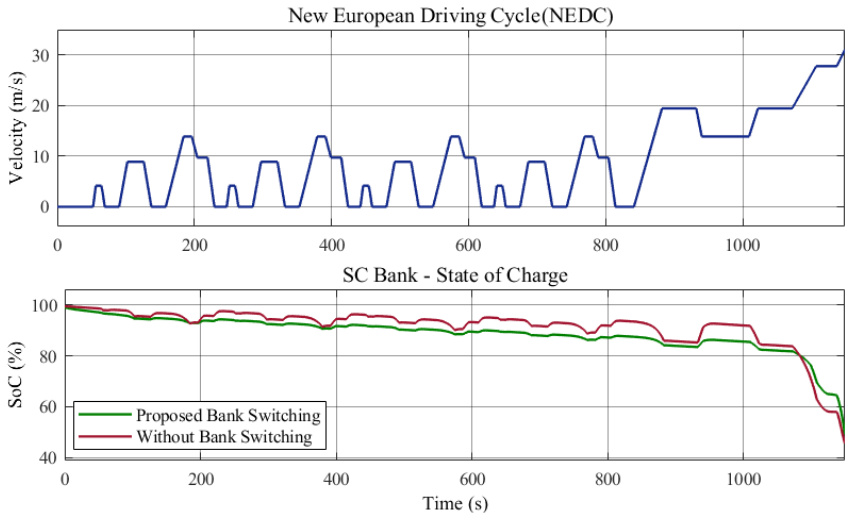

(c)

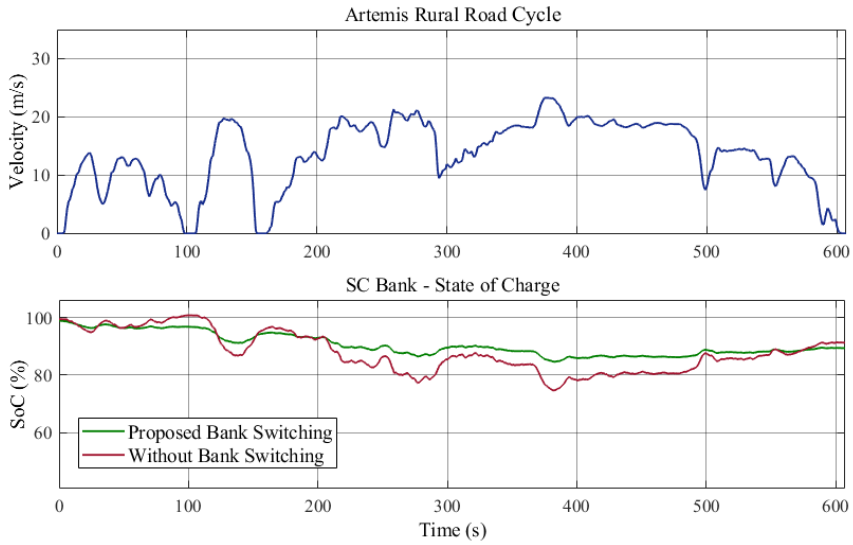

(d)

Figure 5.7. SoC results for (a) UDDS, (b) HWFET, (c) NEDC, (d) Artemis cycles.

However, the proposed SC bank architecture offers higher power delivery duration and assist the battery in delivering more power to the load on a single charge compared to the non-switched SC bank. To verify the power delivery duration of the proposed SC bank in HESS, the simulation studies on the SoC of the SC bank with regard to the aforementioned drive cycles are conducted. The results of the SC bank with and without switching for UDDS, HWFET, NEDC, and Artemis rural driving schedules are shown in Figure 5.7 (a),

(b), (c) and (d) respectively. The results show that the SC bank with the bank switching method offers a high SoC in comparison to the SC bank without any switching during the discharge process. This implies that the proposed configuration enhances the power delivery duration and serves more transient power demands without further recharging through batteries.

5.5.3. Depth of Discharge

The DoD analysis of the SC banks for various drive cycles is performed and the results are summarized in Figure 5.8.

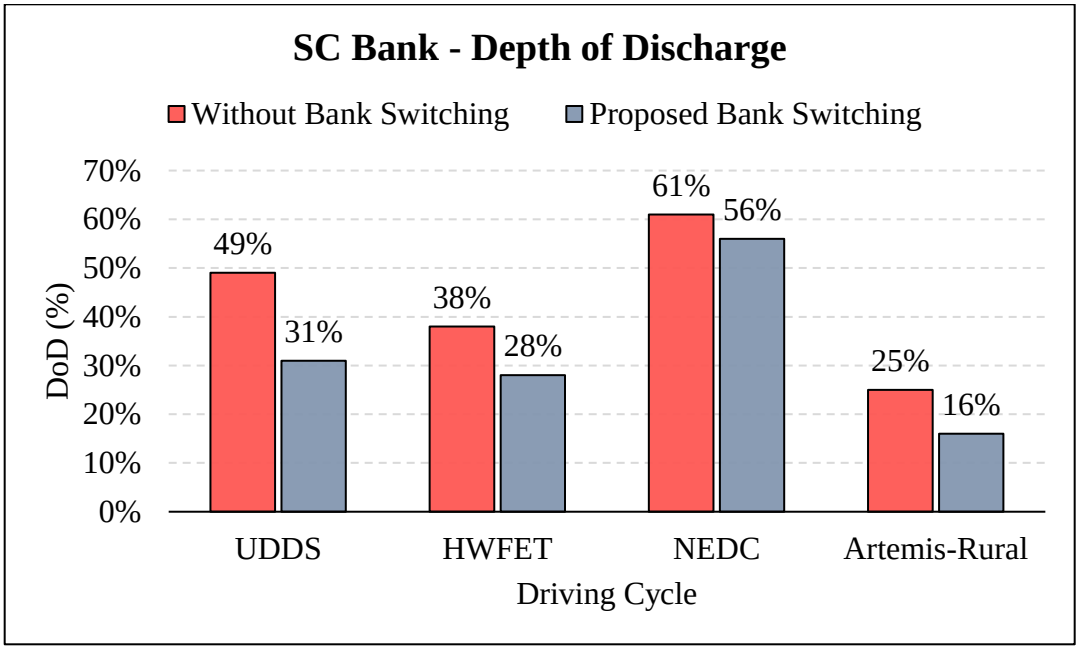

Figure 5.8. DoD of the SC bank under various drive cycles.

It is observed that the DoD of the SC bank for the Artemis-rural drive cycle is low compared to the other drive patterns. Whereas the NEDC driving pattern consumes 61% of the SC bank throughout the cycle. Nevertheless, the proposed configuration offers a parallel to a series transition that provides high capacitance and allows lower discharge rates. Hence, the proposed SC switching architecture is reliable in dealing with a series of transient pulses for a longer duration compared to the SC bank without any switching.

5.6. Summary

The real-time studies of the proposed SC bank in HESS are performed on an EV under four different driving patterns to verify the suitability of the proposed switching circuit in the HESS applications. The drive cycle results justify that the terminal voltage variation of the proposed SC bank is limited to 36% and with an average reduction of 30% compared to the non-switched SC bank. Moreover, it offers a lower DoD around a 15% reduction. As a result, it reduces the stress on batteries and enhances the range of the EV.

Chapter 6

Conclusions

The thesis focusses on introducing a new and simple bank switching architecture termed as auxiliary bank switching of SCs. The proposed architecture enhances the cell energy utilization and power delivery duration of the SC bank with controlled terminal voltage variations during the discharge operation. Chapter 1 provides an overview of batteries and SC energy storage focusing on electric vehicular applications. Moreover, a detailed introduction on hybrid energy storage systems and various power converter topologies to interface the batteries and SCs to drive an electric propulsion system is discussed. Moving forward, a literature review on several traditional bank switching techniques and their merits and demerits were presented. It is noticed that conventional methods have numerous disadvantages in terms of SC cell energy utilization, power delivery duration, and terminal voltage variations. Besides, the switch count and complexity of the SC bank switching rise exponentially with the sizing level of an SC bank.

Addressing these issues, Chapter 2 introduces a new auxiliary bank switching topology with the reduced complexity and improved power delivery duration of the SC banks. A simple control scheme is implemented to switch the auxiliary bank with respect to the terminal voltage of the bank. The simulations and experimental analysis of charge and discharge of SC bank using the proposed switching scheme is implemented. The results show that the energy utilization of each SC cell is 23% high compared to the SC cells in a bank without any switching. On the other hand, the loss analysis is performed that shows the system efficiency of the proposed circuit reaches 92%. Moreover, the cost analysis on the non-switched SC bank, conventional SC bank, and the proposed SC bank shows that the cost of the new circuit is 25% less than the traditional ones.

The later chapter describes a bidirectional dc-dc power converter and control during the discharge of the SC bank to deliver a constant voltage. Inductor current of the current is considered and a comparative analysis on non-switched SC bank and proposed SC bank is performed. The current variation of the inductor in the proposed method is less compared

to a non-switched SC bank. This helps in designing the inductor with reduced current ratings. Thus, the cost of the bidirectional power converter is reduced.

Based on the analysis from the previous chapters, the proposed SC bank with a bidirectional dc-dc power converter is further integrated with a battery to form a HESS. A detailed case study on a small EV employed with the proposed HESS is conducted under four different driving cycles that include UDDS, HWFET, NEDC, and Artemis rural drive cycle. The results show that the voltage variations of the proposed SC bank are constant and are maintained at 36%. On the other hand, the DoD of the new SC bank is highly reduced and offers high power delivery time to serve more load transients in a single charge, in which it reduces the burden on the battery pack of the HESS.

Overall, the proposed architecture can be implemented without a power converter for an application that permits <36% of terminal voltage variations i.e. for instance, the line-voltage regulation. Moreover, this topology enhances the driving range of an EV, if employed in the HESS application for the mass transit buses and other heavy traction applications. They assist the battery pack in serving the transient demands. However, they cannot reach the energy densities of the Li-ion battery packs. Where the upcoming new electric energy storage technologies in the near future may resolve this concern.

6.1. Contributions

1. The minimum discharge voltage analysis of SC bank shows that cell energy utilization is relatively low for high power loads. Thus, a new bank switching architecture and a simple control strategy for SCs is proposed in this thesis.
    - The configuration comprises the main and auxiliary SC banks. The design and sizing aspects of these banks are discussed in detail.
    - The proposed architecture and its timely transition enhance the power delivery duration of the bank by 15% and the cell energy utilization by 23% compared to non-switched SC bank. However, a 3% rise in power delivery time is noticed when compared to the conventional bank switching approach.
    - The loss analysis proves that the proposed method has reduced the switching and conduction losses by 49% compared to the conventional method.

- The cost analysis shows that the system cost of the proposed architecture is reduced by 25% compared to the conventional switching method.

2. Simulation models are designed and developed in MATLAB/Simulink, and PLECS platforms to verify the concept. Besides, a scaled-down hardware prototype with an op-amp based analog controller is developed to validate the proposed method.
3. The impact of bank switching on a bidirectional dc-dc converter is examined and the analysis shows a 55% reduction in the current stress on an inductor in comparison to the SC bank without any switching.
4. To verify the suitability of the proposed SC bank, a case study on HESS based EV is conducted and verified for UDDS, HWFET, NEDC, and Artemis drive cycles.
    - The proposed switching control maintains the SC bank terminal voltage variations within 36% for all four driving patterns.
    - The SoC of the proposed SC bank is monitored which shows an average decrease in DoD of the SC bank by 15%.

6.2. Future Work

1. To verify the suitability of the proposed SC bank, a hardware prototype of battery-SC based HESS can be implemented and tested for other driving schedules.
2. The proposed concept is verified in this work by employing a half-bridge bidirectional dc-dc converter with SC bank. The studies can be further explored by implementing other power electronic converters such as Cuk converter, full-bridge bidirectional dc-dc converters, etc.
3. The performance of SCs in the present work is studied by excluding the degradation and aging effects. These factors can be considered to analyze the effectiveness of an SC bank for variable power loads.
4. A simplified first-order SC model is employed in this work. Further studies on implementing newer models with dynamic behavior may produce precise results.
5. A frequency-based power allocation technique is used in this study to allocate the load power between batteries and SCs. However, various advanced power allocation techniques such as Fast Fourier Transform (FFT) based HESS control can be explored.

Appendix A. Experimental Setup

A1. Non-Switched Supercapacitor bank.

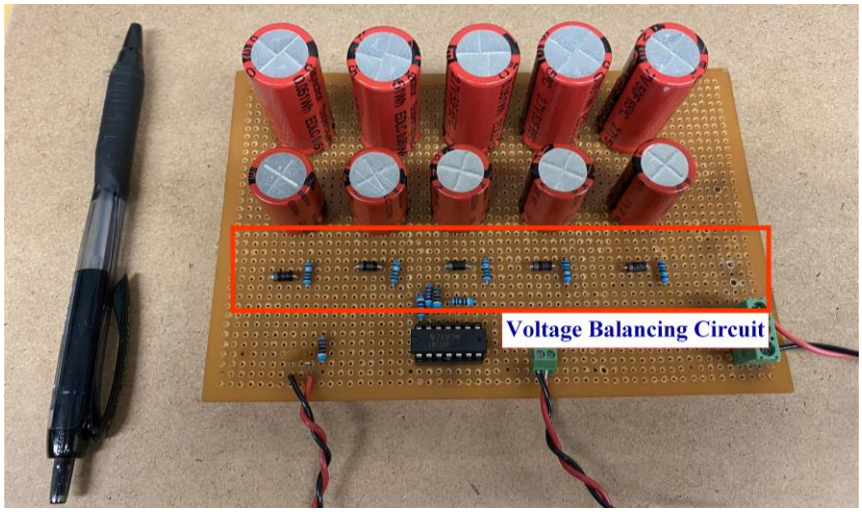

Figure A1. Supercapacitor bank without any switching circuit.

A2. Supercapacitor bank with the proposed switching circuit.

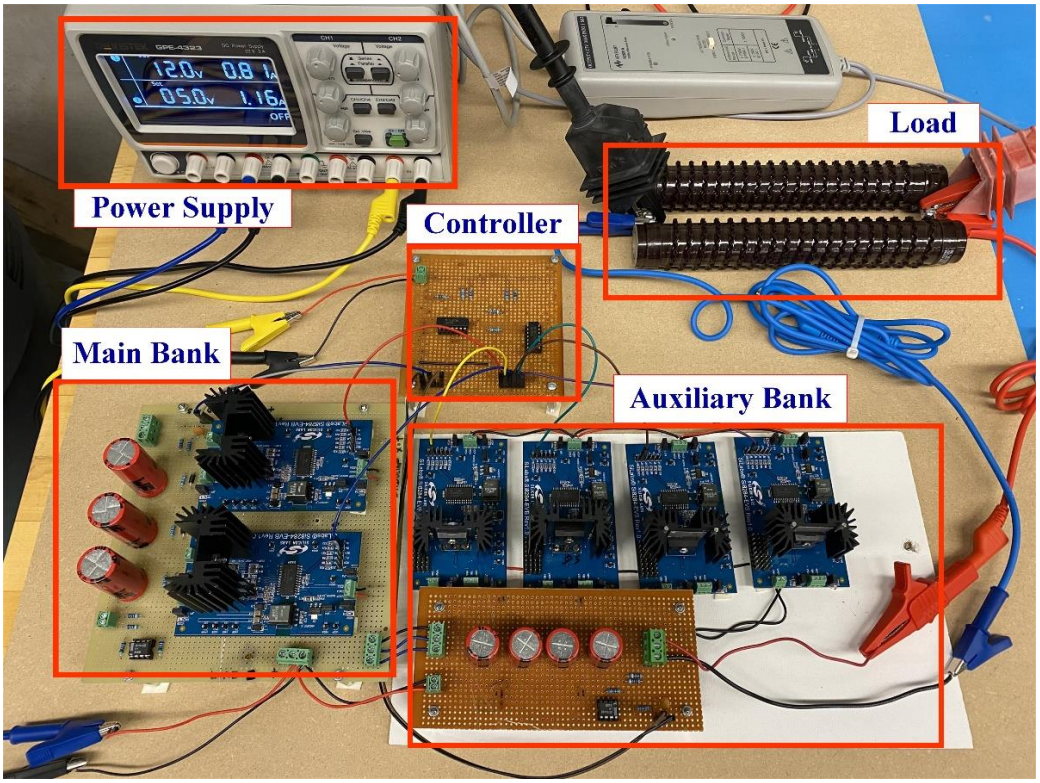

Figure A2. Supercapacitor bank with the proposed switching circuit.

Bibliography

[1]. "Greenhouse gas sources and sinks: executive summary 2017," *ES.5 Canadian economic sectors*.

[2]. D. Zhu and Y. A. Zhang, "Optimal Coordinated Control of Multiple Battery Energy Storage Systems for Primary Frequency Regulation," *IEEE Trans. on Power Sys.*, vol. 34, no. 1, pp. 555-565, Jan. 2019.

[3]. G. Kujundžić, M. Vašak, and J. Matuško, "Estimation of VRLA battery states and parameters using Sigma-point Kalman filter," in *Proc. International Conf. on Electric. Drives and Power Electron. (EDPE)*, Tatranska Lomnica, 2015, pp. 204-211.

[4]. S. Manzetti and F. Mariasiu, "Electric vehicle battery technologies: From present state to future systems," *Renew. Sustain. Energy Rev.*, vol. 51, pp. 1004–1012, Nov. 2015.

[5]. M. A. Hannan, M. M. Hoque, A. Hussain, Y. Yusof and P. J. Ker, "State-of-the-Art and Energy Management System of Lithium-Ion Batteries in Electric Vehicle Applications: Issues and Recommendations," *IEEE Access*, vol. 6, pp. 19362-19378, 2018.

[6]. Q. Yu, R. Xiong, C. Lin, W. Shen, and J. Deng, "Lithium-Ion Battery Parameters and State-of-Charge Joint Estimation Based on H-infinity and Unscented Kalman Filters," *IEEE Trans. on Vehi. Tech.*, vol. 66, no. 10, pp. 8693-8701, Oct. 2017.

[7]. S. Al-Hallaj, R. Kizilel, A. Lateef, R. Sabbah, M. Farid, and J. R. Selman, "Passive thermal management using phase change material (PCM) for EV and HEV Li-ion batteries," in *Proc. IEEE Veh. Power and Propul. Conf.*, Chicago, IL, 2005, pp. 5 pp.

[8]. M. Chen and G. A. Rincon-Mora, "Accurate, Compact, and Power-Efficient Li-Ion Battery Charger Circuit," *IEEE Trans. on Circuits and Systems II: Express Briefs*, vol. 53, no. 11, pp. 1180-1184, Nov. 2006.

[9]. K. Thirugnanam, H. Saini and P. Kumar, "Mathematical modeling of Li-ion battery for charge/discharge rate and capacity fading characteristics using genetic algorithm approach," in *Proc. IEEE Transport. Electrific. Conf. and Expo (ITEC)*, Dearborn, MI, 2012, pp. 1-6.

[10]. I. Husain, “Electric and Hybrid Vehicles-Design Fundamentals,” *CRC Press*, ISBN 0-8493-1466-6, 2003.

[11]. Lijun Gao, R. A. Dougal, and Shengyi Liu, “Power enhancement of an actively controlled battery/ultracapacitor hybrid,” *IEEE Trans. Power Electron.*, vol. 20, no. 1, pp. 236–243, Jan. 2005.

[12]. A. Ostadi and M. Kazerani, “A Comparative Analysis of Optimal Sizing of Battery-Only, Ultracapacitor-Only, and Battery-Ultracapacitor Hybrid Energy Storage Systems for a City Bus,” *IEEE Trans. Veh. Technol.*, vol. 64, no. 10, pp. 4449–4460, Oct. 2015.

[13]. D. Ronanki, S. A. Singh and S. S. Williamson, “Comprehensive Topological Overview of Rolling Stock Architectures and Recent Trends in Electric Railway Traction Systems,” *IEEE Trans. Transport. Electrific.*, vol. 3, no. 3, pp. 724–738, Sept. 2017.

[14]. J. Rocabert, R. Cap-Misut, R. S. Muoz-Aguilar, J. I. Candela and P. Rodriguez, “Control of Energy Storage System Integrating Electrochemical Batteries and Supercapacitors for Grid-Connected Applications,” *IEEE Trans. Ind. Appl.*, vol. 55, no. 2, pp. 1853–1862, March-April 2019.

[15]. A. Misra, “Energy Storage for Electrified Aircraft: The Need for Better Batteries, Fuel Cells, and Supercapacitors,” *IEEE Electrific. Mag.*, vol. 6, no. 3, pp. 54–61, Sept. 2018.

[16]. T. Kwon, S. Lee, S. Sul, C. Park, N. Kim, B. Kang, and M. Hong, “Power control algorithm for hybrid excavator with supercapacitor,” *IEEE Trans. Ind. Appl.*, vol. 46, no. 4, pp. 1447–1455, Jul. 2010.

[17]. D. Ronanki and S. S. Williamson, "New modulation scheme and voltage balancing control of modular multilevel converters for modern electric ships," *IET Power Electron.*, vol. 12, no. 13, pp. 3403-3410, 2019.

[18]. P. Thounthong, “Model based energy control of a solar power plant with a supercapacitor for grid independent applications,” *IEEE Trans. Energy Convers.*, vol. 26, no. 4, pp. 1210–1218, Dec. 2011.

[19]. A. Ghazanfari, M. Hamzeh, H. Mokhtari, and H. Karimi, “Active Power Management of Multihybrid Fuel Cell/Supercapacitor Power Conversion System in

a Medium Voltage Microgrid," *IEEE Trans. Smart Grid*, vol. 3, no. 4, pp. 1903–1910, Dec. 2012.

[20]. C. Abbey and G. Joos, "Supercapacitor Energy Storage for Wind Energy Applications," *IEEE Trans. Ind. Appl.*, vol. 43, no. 3, pp. 769-776, May–June 2007.

[21]. H. Yang, "Bounds of supercapacitor open-circuit voltage change after constant power experiments," in *Proc. of the 10th Electric. Energy Storage Appli. and Tech. (EESAT 2017)*, 2017, pp. 1–5.

[22]. S. S. Williamson, A. Khaligh, Sung Chul Oh, and A. Emadi, "Impact of energy storage device selection on the overall drive train efficiency and performance of heavy-duty hybrid vehicles," in *Proc. IEEE Vehicle Power and Propul. Conf.*, Chicago, IL, 2005, pp. 1-10.

[23]. A. M. O. Haruni, M. Negnevitsky, M. E. Haque, and A. Gargoom, "A Novel Operation and Control Strategy for a Standalone Hybrid Renewable Power System," *IEEE Trans. on Sustain. Energy*, vol. 4, no. 2, pp. 402-413, April 2013.

[24]. S. C. Lee & O. Kwon, S. Thomas, S. Park, and G. Choi, "Graphical and mathematical analysis of fuel cell/battery passive hybridization with K factors," *Applied Energy*. 114. 135-145, February 2014.

[25]. D. Shin, Y. Kim, J. Seo, N. Chang, Y. Wang and M. Pedram, "Battery-supercapacitor hybrid system for high-rate pulsed load applications," in *Proc. Design, Automation & Test in Europe*, Grenoble, 2011, pp. 1-4.

[26]. S. Vazquez, S. M. Lukic, E. Galvan, L. G. Franquelo and J. M. Carrasco, "Energy Storage Systems for Transport and Grid Applications," *IEEE Trans. Ind. Electron.*, vol. 57, no. 12, pp. 3881‑3895, Dec. 2010.

[27]. Q. Zhang and G. Li, "Experimental Study on a Semi-Active Battery-Supercapacitor Hybrid Energy Storage System for Electric Vehicle Application," *IEEE Trans. Power Electron.*, vol. 35, no. 1, pp. 1014-1021, Jan. 2020.

[28]. S. Sugimoto, S. Ogawa, H. Katsukawa, H. Mizutani, M. Okamura, "A Study of Series-Parallel Changeover Circuit of a Capacitor Bank for an Energy Storage System Utilizing Electric Double-Layer Capacitors," *Electr. Eng. in Japan*, vol. 145, no. 3, pp. 34–42, 2003.

[29]. M. Uno and H. Toyota, “Supercapacitor-based energy storage system with voltage equalizers and selective taps,” in *Proc. IEEE Power Electron. Spec. Conf.*, Rhodes, 2008, pp. 755–760.

[30]. X. Fang, N. Kutkut, J. Shen, I. Batarseh, “Analysis of generalized parallel-series ultracapacitor shift circuits for energy storage systems,” *Renewable Energy*, vol. 36, pp. 2599–2604, 2011.

[31]. M. Uno and K. Tanaka, “Unregulated interface converter based on cascaded switched capacitor converters for supercapacitors in alternative battery applications,” in *Proc. IEEE Int. Conf. on Power Electron. And Drive Sys.*, Singapore, 2011, pp. 579-586.

[32]. J. Nie, X. Xiao, Z. Nie, P. Tian, and R. Ding, “A novel three-level changeover circuit of super-capacitor bank for energy storage systems,” in *Proc. 38th Annu. Conf. of the IEEE Ind. Electron. Soc.*, Montreal, QC, 2012, pp. 144–149.

[33]. N. Sidhu, L. Patnaik, N. A. Azeez, and S. S. Williamson, “Bank Switching Technique in Supercapacitor Energy Storage Systems for Line Voltage Regulation in Pulsed Power Applications,” in *Proc. 44th Annu. Conf. of the IEEE Ind. Electron. Soc.*, Washington, DC, 2018, pp. 5027–5031.

[34]. N. Khan, N. Mariun, M. Zaki, and L. Dinesh, “Transient analysis of pulsed charging in supercapacitors,” in *Proc. IEEE TENCON*, vol. 3, Sept. 2000, pp. 193- 199.

[35]. G.C. Ballard, H.B. Sierra-Alcazar, H.L. Lee, and J.L. Morris, “Operating principles of the ultracapacitor,” *IEEE Trans. Magn.*, vol. 25, pp. 102-106, Jan. 1989.

[36]. H. Yang and Y. Zhang, “Self-discharge analysis and characterization of supercapacitor for environmentally powered wireless sensor network applications,” *J. Power Sources*, vol. 196, pp. 8866-8873, Oct. 2011.

[37]. “Datasheet, Bootscap Ultracapacitors,” *Maxwell Technologies*, Tech. Rep. Doc. No. 1009364 Rev.3, 2009.

[38]. O. Onar and A. Khaligh, “Dynamic modeling and control of a cascaded active battery/ultra-capacitor based vehicular power system,” in *Proc. IEEE Vehicle Power and Propulsion Conf.*, Harbin, 2008, pp. 1-4.

[39]. MATLAB/Simulink model, “Implement generic supercapacitor model,” *The MathWorks Inc.*, 2013.

[40]. A. S. Kirtiwar, “Ultracapacitor Charging Methods,” *International Research Journal of Engineering and Technology (IRJET)*, vol. 3, no. 2, Feb. 2016.

[41]. F. Puhane, R. Kalbitz “How to Use Supercapacitors - A Brief Guide to the Design-In Process,” *Würth Elektronik*, Doc.No SN009a, 2019.

[42]. K. Maneesut and U. Supatti, “Reviews of supercapacitor cell voltage equalizer topologies for EVs,” in *Proc. 14th International Conf. on Electri. Eng./Electron., Computer, Telecom. and Info. Tech. (ECTI-CON)*, Phuket, 2017, pp. 608-611.

[43]. D. Linzen, S. Buller, E. Karden and R. W. De Doncker, “Analysis and evaluation of charge-balancing circuits on performance, reliability, and lifetime of supercapacitor systems,” *IEEE Trans. Ind. Appl.*, vol. 41, no. 5, pp. 1135-1141, Sept.-Oct. 2005.

[44]. D. Linzen, S. Buller, E. Karden and R. W. De Doncker, “Analysis and evaluation of charge-balancing circuits on performance, reliability, and lifetime of supercapacitor systems,” *IEEE Trans. Ind. Appl.*, vol. 41, no. 5, pp. 1135–1141, Sept.-Oct. 2005.

[45]. L. C. Rosario, J. T. Economou, and P.C.K.Luk, “Short Interval Supercapacitor Switching Networks for Electric Vehicles: A Parametric Approach,” *IEEE International Vehi. Power and Propul. Conf.*, VPP04, Paris, France, 2004.

[46]. H. Wu, P. Xu, H. Hu, Z. Zhou and Y. Xing, “Multiport Converters Based on Integration of Full-Bridge and Bidirectional DC–DC Topologies for Renewable Generation Systems,” *IEEE Trans. Ind. Electron.*, vol. 61, no. 2, pp. 856-869, Feb. 2014.

[47]. A. S. Samosir and A. H. M. Yatim, “Implementation of Dynamic Evolution Control of Bidirectional DC–DC Converter for Interfacing Ultracapacitor Energy Storage to Fuel-Cell System,” *IEEE Trans. Ind. Electron.*, vol. 57, no. 10, pp. 3468-3473, Oct. 2010.

[48]. K. A. Kanhav and M. A. Chaudhari, “A bidirectional multiport dc-dc converter topology for hybrid energy system,” in *Proc. International Conf. on Energy, Communication, Data Analytics, and Soft Computing (ICECDS)*, Chennai, 2017, pp. 3427-3432.

[49]. Z. Amjadi and S. S. Williamson, "Power-Electronics-Based Solutions for Plug-in Hybrid Electric Vehicle Energy Storage and Management Systems," *IEEE Trans. on Ind. Electron.*, vol. 57, no. 2, pp. 608-616, Feb. 2010.

[50]. J. Cao and A. Emadi, "A New Battery/UltraCapacitor Hybrid Energy Storage System for Electric, Hybrid, and Plug-In Hybrid Electric Vehicles," *IEEE Trans. on Power Electron.*, vol. 27, no. 1, pp. 122-132, Jan. 2012.

[51]. D. Stroe, M. Swierczynski, S. K. Kær, E. M. Laserna, and E. S. Zabala, "Accelerated aging of Lithium-ion batteries based on electric vehicle mission profile," in *Proc. IEEE Energy Conver. Congr. and Expo. (ECCE)*, Cincinnati, OH, 2017, pp. 5631-5637.

[52]. N. Omar, M. Daowd, O. Hegazy, P. Van den Bossche, T. Coosemans, J. Van Mierlo, "Electrical Double-Layer Capacitors in Hybrid Topologies - Assessment and Evaluation of Their Performance," *Energies*, vol. 5, pp. 4533-4568, Nov. 2012.

[53]. F. Naseri, E. Farjah, and T. Ghanbari, "An Efficient Regenerative Braking System Based on Battery/Supercapacitor for Electric, Hybrid, and Plug-In Hybrid Electric Vehicles With BLDC Motor," *IEEE Trans. Vehi. Tech.*, vol. 66, no. 5, pp. 3724-3738, May 2017.

[54]. D. Ronanki and S. S. Williamson, "Modular Multilevel Converters for Transportation Electrification: Challenges and Opportunities," *IEEE Trans. Transport. Electrific.*, vol. 4, no. 2, pp. 399-407, June 2018.

[55]. S. Lu, K. A. Corzine, and M. Ferdowsi, "A New Battery/Ultracapacitor Energy Storage System Design and Its Motor Drive Integration for Hybrid Electric Vehicles," *IEEE Trans. Vehi. Tech.*, vol. 56, no. 4, pp. 1516-1523, July 2007.

[56]. M. B. Camara, H. Gualous, F. Gustin and A. Berthon, "Design and New Control of DC/DC Converters to Share Energy Between Supercapacitors and Batteries in Hybrid Vehicles," *IEEE Trans. Vehi. Tech.*, vol. 57, no. 5, pp. 2721-2735, Sept. 2008.

[57]. A. Khaligh and Z. Li, "Battery, Ultracapacitor, Fuel Cell, and Hybrid Energy Storage Systems for Electric, Hybrid Electric, Fuel Cell, and Plug-In Hybrid Electric Vehicles: State of the Art," *IEEE Trans. Vehi. Tech.*, vol. 59, no. 6, pp. 2806-2814, July 2010.

[58]. R. Carter, A. Cruden, and P. J. Hall, “Optimizing for Efficiency or Battery Life in a Battery/Supercapacitor Electric Vehicle,” *IEEE Trans. Vehi. Tech.*, vol. 61, no. 4, pp. 1526-1533, May 2012.

[59]. H. Xiaoliang, T. Hiramatsu, and H. Yoichi, “Energy Management Strategy based on frequency-varying filter for the battery supercapacitor hybrid system of Electric Vehicles,” in *Proc. World Electric Vehicle Symposium and Exhibition (EVS27)*, Barcelona, 2013, pp. 1-6.

[60]. Z. Li, O. Onar, A. Khaligh, and E. Schaltz, “Design, control, and power management of a battery/ultra-capacitor hybrid system for small electric vehicles,” in *Proc. SAE World Congr. Exh.*, Detroit, MI, Apr. 2009, doc. No. 2009-01-1387.